MOLECULAR DYNAMICS STUDIES ON MANIPULATION OF SURFACE WETTING USING NANOSCALE SURFACE STRUCTURES

A Thesis Submitted to
the Graduate School of Engineering and Science of
İzmir Institute of Technology
in Partial Fulfillment of the Requirements for the Degree of

MASTER OF SCIENCE

in Mechanical Engineering

by
Hüseyin Gökberk ÖZÇELİK

July 2019
İZMİR

We approve the thesis of **Hüseyin Gökberk ÖZÇELİK**

Examining Committee Members:

Assoc. Prof. Dr. Murat BARIŞIK
Department of Mechanical Engineering, İzmir Institute of Technology

Assoc. Prof. Dr. Erdal ÇETKİN
Department of Mechanical Engineering, İzmir Institute of Technology

Assist. Prof. Dr. Hasan ÇELİK
Department of Mechanical Engineering, İzmir University of Economics

19 July 2019

Assoc. Prof. Dr. Murat BARIŞIK
Supervisor, Department of Mechanical Engineering, İzmir Institute of Technology

Prof. Dr. Sedat AKKURT
Head of the Department of Mechanical Engineering

Prof. Dr. Aysun SOFUOĞLU
Dean of the Graduate School of Engineering and Sciences

ACKNOWLEDGMENTS

I would like to express my profound gratitude to my advisor Assoc. Prof. Murat BARIŞIK who has kept me motivated during my days in MiNaEng and had patience to cope with my countless questions and concerns. He provided me excellent research opportunities and he has always shared his previous experiences and knowledge. I am sincerely thankful to him for his support and guidance.

I am thankful to Prof. Ali BEŞKÖK for his valuable contributions to my research during this study. Also, I would like to thank to Center for Scientific Computation at Southern Methodist University for allowing us to use their high-performance computing center, ManeFrame. And, I would like to thank to Turkish National e-Science e-Infrastructure (TRUBA) for providing us computational infrastructure to conduct the research.

I am thankful to Assoc. Prof. Hasan ŞAHİN and Yiğit SÖZEN for their solid contributions on ab initio simulations. This work would be incomplete without their contributions. Also, I am thankful to Assoc. Prof. Haldun SEVİNÇLİ for introducing me ab initio calculations and for his valuable comments on ab initio simulations.

It is a great pleasure to be part of MiNaEng Research Group. I would like to acknolwedge my sincere gratitude to my colleagues from the research group. Particularly, I would genuinely like to thank Safa SABET and Gülce KALYONCU for their friendship and support.

We would like to thank The Scientific and Technological Research Council of Turkey (TUBITAK), for giving us the opportunity to carry out this research. This work is supported by TUBITAK under the grant number TÜBİTAK 217M460.

I would like to send my most sincere gratefulness to my family, my mother Sabire ÖZÇELİK, my father İsmail ÖZÇELİK and my sister Gülşah ÖZÇELİK. They have always believed in me and encouraged me to reach further. They have supported me in every decision I have made. I would never have been able to finish this work without their supports and encouragement.

I would like to express my greatest appreciations to my fiancé Hilal Cihankaya who has always had patience to tolerate my stubbornness. She has never stoped supporting me. I am grateful to her for limitless support and continuous love.

ABSTRACT

MOLECULAR DYNAMICS STUDIES ON MANIPULATION OF SURFACE WETTING USING NANOSCALE SURFACE STRUCTURES

The discovery of the lotus effect relating to the hydrophobic nature of lotus leaves is significant to surface structures on wetting. By considering the lotus effect, efforts have been made to mimics the effect of surface stuctures to manipulate wetting and surface patterning is introduced to capture underlying mechanism of lotus effect. Later, the effect of nanosized structures on rose petals is also addressed. Interestingly, while both lotus leaf and rose petal show hydrophobic behavior, due to nanosized structures, rose petals exhibit sticky behavior in contrast to the slippery lotus leaves. Herein, to investigate the effect of nanosized surface structures on wetting, molecular dynamics studies on wetting of nanopatterned silica surfaces are performed. Before performing wetting studies on the surfaces, ab initio based calcuations and molecular dynamics studies are conducted to assure modelled surfaces capture wetting behavior of silica surfaces and it is found that ab inito based calculations overestimate the interactions between water and silica surfaces. Consequently, parametric molecular dynamics studies are performed and force field parameters capturing wetting behavior of silica surfaces are proposed. Then, two different silica surfaces are subjected to investigation and applicability of models predicting contact angle is examined. Previous models proposed in the literature fail in predicting contact angle on nanopatterned silica surfaces. Therefore, initially, averaged water density inside the cavity is considered to characterize wetting behavior but significant variation from trendline is observed. Then, non dimensional surface parameter is proposed to capture wetting on nanopatterned silica surfaces and change in the work of adhesion is correlated with non dimensional surface parameter.

Keywords and Phrases: Biomimetic Surfaces, Surface Patterning, Wetting of Nanopatterned Surfaces, Molecular Dynamics

ÖZET

NANO ÖLÇEKLİ YÜZEY YAPILARI KULLANARAK YÜZEY ISLATMA MANİPÜLASYONU ÜZERİNE MOLEKÜLER DİNAMİK ÇALIŞMALARI

Lotus yapraklarının hidrofobik doğası ile ilgili lotus etkisinin keşfi, ıslanma üzerindeki yüzey yapıları için önemlidir. Lotus etkisi göz önünde bulundurularak, ıslatma davranışını manipüle etmek için yüzey yapılarının etkisini taklit etmeye yönelik çabalar gösterilmiştir ve lotus etkisinin altta yatan mekanizmasını yakalamak için yüzey desenleme uygulanır. Daha sonra, nano-boyutlu yapıların gül yaprağı üzerindeki etkisi değinilmiştir. İlginç bir şekilde, hem lotus yaprağı hem de gül yaprağı, nano boyutlu yapılar nedeniyle hidrofobik davranış sergilerken, gül yaprakları kaygan nilüfer yapraklarının aksine yapışkan davranış sergiler. Burada, nano-boyutlu yüzey yapılarının ıslatma üzerindeki etkisini araştırmak için nano-desenlenmiş silika yüzeylerin ıslatılması üzerine moleküler dinamik çalışmaları gerçekleştirilmiştir. Yüzeylerde ıslatma çalışmaları yapılmadan önce, modellenen yüzeylerin silika yüzeylerinin ıslanma davranışını yakalamasını sağlamak için ab initio esaslı hesaplamalar ve moleküler dinamik çalışmaları gerçekleştirilmiştir ve ab inito esaslı hesaplamaların su ve silika yüzey arasındaki etkileşimi yüksek tahmin ettiği bulunmuştur. Dolayısıyla parametrik moleküler dinamik çalışmaları yapılmış ve silika yüzeylerin ıslanma davranışını yakalayan kuvvet alanı parametreleri önerilmiştir. Daha sonra, iki farklı silika yüzeyi araştırmaya tabi tutulmuştur ve temas açısını tahmin edebilen modellerin uygulanabilirliği incelenmiştir. Literatürde önerilen önceki modeller nano desenlenmiş silika yüzeylerde temas açısını tahmin etmekte başarısız olmaktadır. Bu nedenle, başlangıçta, oyuk içindeki ortalama su yoğunluğunun ıslatma davranışını karakterize ettiği düşünülmüştür, ancak trend çizgisinden önemli farklılıklar gözlenmiştir. Daha sonra, nano desenlenmiş silika yüzeylerde ıslanmayı yakalamak için boyutsuz yüzey parametresi önerilmiştir ve adezyon işindeki değişim, boyutsuz yüzey parametresi ile ilişkilendirilmiştir.

Anahtar Kelimeler ve Deyimler: Biyobenzetilmiş Yüzeyler, Yüzey Desenleme, Nano Desenlenmiş Yüzeylerin Islanması, Moleküler Dinamik

TABLE OF CONTENTS

LIST OF FIGURES

Figure **Page**

LIST OF TABLES

LIST OF SYMBOLS

a	Acceleration	m/s^2
f	Surface fraction	
h	Pillar height	nm
r	Distance, roughness ratio	nm,
r(t)	Position	m
s	Distance between periodic pillars	nm
q	Electrostatic charge	e
w	Pillar width	nm
W	Work	N/m
t	Time	s

Greek Letters

ε	Interaction strength, dielectric constant	eV, F/m
θ	Contact angle	deg.
σ	Molecular diameter	Å
γ	Interfacial tension	N/m
τ	Line tension	N
ρ	Density	g/cm^3
ρ^*	Normalized water density inside the cavity	

Subscripts

B	Base
C-B	Cassie-Baxter
G	Gas
L	Liquid
S	Solid
W	Wenzel
∞	Macroscopic droplet

CHAPTER 1

INTRODUCTION

Wetting is an important phenomenon that occurs as a result of adhesive and cohesive forces when three different phases meet. Cohesion is defined as an attractive interaction between similar atoms or molecules. Conversely, adhesion is defined as forces between atoms or molecules of different kinds. When two or more different phases meet on the interface, interfacial tensions occur due to excess energies originating from a force imbalance at the interface. As a result, surface wetting is observed because of the equilibrium in interfacial tensions on a surface. Generally, wetting is quantified by the contact angle and equilibrium between interfacial tensions is described as a function of contact angle by Young's equation[1] which is expressed as follow;

$$\gamma_{SG} = \gamma_{SL} + \gamma_{LG}\cos\theta_{\infty} \tag{1.1}$$

γ stands for interfacial tension and subscripts S, L and G denotes solid, liquid and gas or vapor phases respectively. θ_{∞} describes macroscopic contact angle.

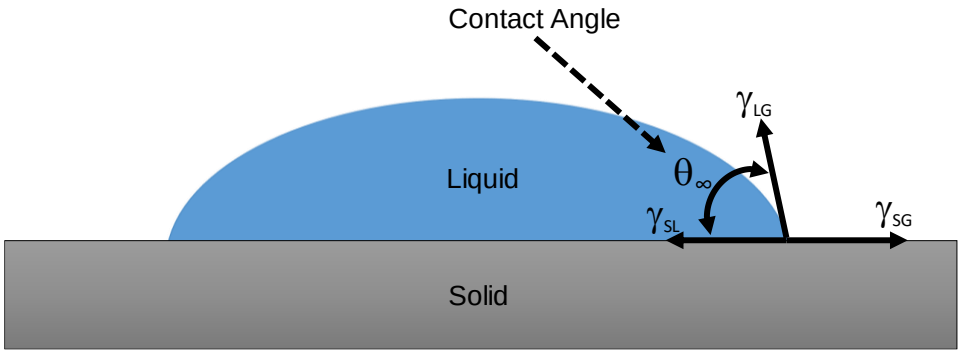

Figure 1.1. Representation of wetting angle and interfacial tensions

In Figure 1.1, illustration of contact angle of a perfectly flat surface and interfacial tensions are presented. Both Young's equation and Figure 1 suggest that contact angle appears as a result of difference in solid-liquid and solid-gas interfacial tensions. When tensions at solid-liquid and solid-gas interfaces are equal, contact angle becomes perpendicular to surface and cos θ_{∞} term vanishes. Moreover, if solid surface has higher tension at the solid-gas interface than solid-liquid interface, the contact angle, θ_{∞}, lies between 0 and $\pi/2$ to assure equilibrium between interfacial tensions. On the contrary, if solid surface has lower tension, the contact angle remains between $\pi/2$ and π. Therefore,

wetting behavior of surfaces can be classified depending on contact angle. For contact angle lower than $\pi/2$ or 90^0, surfaces are called –philic and surfaces that have contact angle higher than $\pi/2$ or 90^0 are called –phobic. When liquid substance is water, the surface is classified as hydrophilic or hydrophobic depending on contact angle. Furthermore, in extremely high contact angle ($>120^0$), surfaces are called superhydrophobic.

Wetting is one of the most fundamental concepts in interfacial phenomena so contact angle plays an important role in a huge number of applications. For example, hydrophilic surfaces are more resistant to fogging because hydrophobic surfaces allow water to form a droplet and fogging occurs. Hydrophilic surfaces prevent fogging by spreading water uniformly on the surface[2]. Similarly, hydrophilic surfaces can also prevent adhesion of unwanted agents, known as fouling, by forming a hydration layer [3]. Moreover, as wetting increases, boiling heat transfer increases so higher heat transfer performance can be obtained on hydrophilic surfaces[4].

Hydrophobic/superhydrophobic surfaces are also desired depending on the application. One of the most advantageous characteristic of hydrophobic surfaces is self-cleaning. Since a water droplet easily slides on hydrophobic surfaces, dust particles can be removed by sliding particles. Similarly, due to the sliding of water droplets, icing on a surface could be eliminated. Moreover, superhydrophobic surfaces can be beneficial in drag reduction for both laminar and turbulent flows[5].

Apart from hydrophobicity or hydrophilicity related applications, wetting gives insight of coupled surface-water interactions so wetting behavior of surfaces can be used as a surface characterization method[6]. Specifically, in microfluidics, as size decreases, surface forces dominate mass/volume forces due to increasing surface to volume ratio. Therefore, efforts have been made to link wetting to micro/nanoscale phenomena such as temperature jump[7] and slip length[8–11]. For these reasons, understanding wetting is essential for surface related engineering applications.

1.1. Wetting Manipulation and Surface Patterning

Since the wetting behavior of solids has great importance for a wide range of applications, from macro- to nano-scale, such as ice/fog formations on a surface, fluid transport inside a channel/tube, and heat conduction from a surface to a fluid, being able

to manipulate wetting can control those mechanisms. To accomplish manipulation, the main objective is to set the tension between surface and other substances and adjust it for desired characteristic. Previous research attempted to adjust surface wetting using coatings or chemicals but with the discovery of the lotus effect, surface patterning has become a promising tool for wetting control.

Lotus flower is attributed to cleanliness and purity in Asian cultures because of the self-cleaning characteristics and hydrophonic nature of its leaves as studied by Barthlott and Neinhuis[12]. The hydrophobicity is linked to micro scale surface structures and lotus effect is defined as a water repellency originating from surface structures. With the discovery of lotus effect, surface patterning has started being implemented to manipulate wetting behavior of surfaces.

The discovery of lotus effect has influenced surface structures on wetting of surfaces and models have been developed to predict the contact angle of structured surfaces. Fundamentally, two different approaches are followed to predict contact angle of rough surfaces. The Wenzel[13] approach assumes water penetrates cavities which appears as a result of surface roughness or surface structures. On the contrary, the Cassie and Baxter[14] (C-B) model assumes that water stays on the surface structures and the penetreation of water molecules into roughness cavities is avoided. A schematical illustration of these models is presented in Figure 1.2.

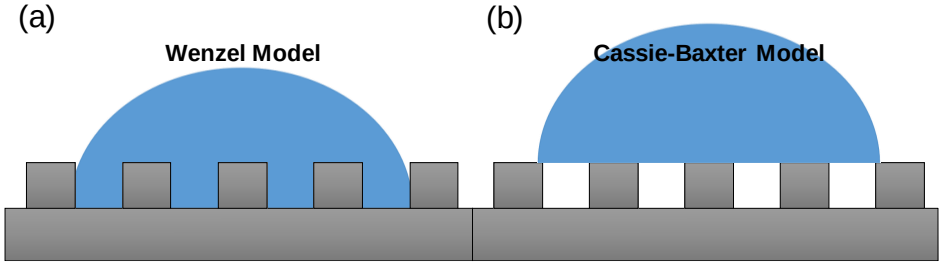

Figure 1.2. Representation of wetting models predicting contact angle depending on surface structures

Both models correlate interfacial tensions to interfacial areas and predict wetting of rough surface by considering geometrical roughness parameters. More specifically, the Wenzel model introduces the term roughness ratio, r, and roughness ratio defines ratio of solid-liquid interfacial area to projected area. Similarly, C-B model introduces the parameter f, surface fraction, to distinguish solid-liquid and gas-liquid interface. Surface fraction is simply ratio of solid-liquid interfacial area to projected area. It should be

underlined that roughness ratio of the Wenzel model should be greater that one and the surface fraction of C-B model should be less than one.

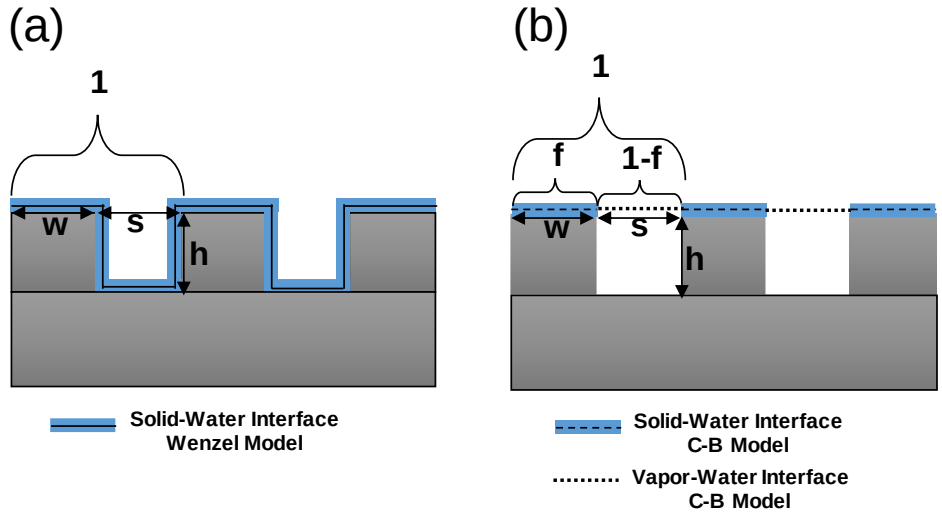

Figure 1.3. Illustration of near Interface region (a) Wenzel model and (b)Cassie-Baxter model

Near interface regions of the two models are shown in Figure 1.3. The blue thick line represents water near the interface region and thin lines denote different interfacial regions. Solid, dashed and dotted lines represent solid-liquid interfacial region of Wenzel state, solid-liquid interfacial region of C-B state and vapor liquid interface of C-B state, respectively. Repeating structure on the surface is specified as 1. Moreover, width, height and cavity width of surface structures are denoted with w, h and s in the Figure 1.3. Roughness ratio and surface fraction of nanogroove as presented in Figure 1.3 are shown in equation 1.2 and 1.3, respectively.

$$r = \frac{w + 2h + s}{s + w} \tag{1.2}$$

$$f = \frac{s}{s + w} \tag{1.3}$$

In the literature, Wenzel state is also called as homogeneous wetting and C-B state is considered as heterogenous wetting because it is assumed that roughness cavities are filled with air and air pockets inside the cavities prevent peneteration of water. Thus, two different interfaces occur between the droplet and surface. On top of the pillar solid-liquid interface occur, and over the cavities liquid-gas interface appears. Presence of liquid gas interface over the cavities increases contact angle of rough surface so C-B state is generally desired for hydrophobic applications on patterned surfaces. Theoretically,

hydrophilic smooth surface can be tuned to be hydrophobic by appliying surface patterning; on the other hand, in Wenzel state, it is theoretically impossible to change hydrophilic surface to hydrophobic with the help of surface patterning. Contact angle predictions according to Wenzel and Cassie-Baxter models are presented in equation 1.4 and 1.5, respectively.

$$\cos\theta_W = r\cos\theta \tag{1.4}$$

$$\cos\theta_{C-B} = \sum_i r f_i \cos\theta_i \tag{1.5}$$

Subscripts W and C-B from equation 1.4 and 1.5 represent Wenzel and Cassie-Baxter states and θ denotes contact angle of smooth surfaces. The term r refers to roughness ratio of wetted area. It should be noted that when only one surface fraction, f equals to one and Cassie-Baxter equation reduces Wenzel equation. Cassie-Baxter model considers contact angle of composite surface as linear combination of contact angles of each fraction so Cassie-Baxter model is also used in predicting contact angle of chemically heterogeneous striped surfaces[15].Similarly, on rough surfaces, contact angle of liquid-gas interface is assumed to 180^0 and Cassie-Baxter equation reduces to;

$$\cos\theta_{C-B} = \cos\theta + f - 1 \tag{1.6}$$

Although Cassie-Baxter and Wenzel models consider single roughness, in nature dual scale roughness is observed commonly. Specifically, the importance of nanoscale roughness on wetting of rose petals is presented.[16] With the discovery of rose petal effect, effect of nanoscale roughness on wetting harnesses attentions to explain wetting behavior of surfaces. Although both surfaces of lotus leaf and rose petal show hydrophobic behavior, surface of rose petal is highly adhesive and sticky behavior of water droplets is observed in contrast to slippery lotus leaf. Researchers attribute sticky behavior on rose petals to nanoscale roughnness of the petal and wetting mechanism of the petal is explained as follows; hydrophobic nature of rose petal originates from microscale roughness and water molecules stay on top of pillars in microscale but sticky behavior is observed because water molecules fill cavities in nanoscale and nanoscale scale roughness prevents slip of water droplets.

Introducing nanoscale roughness to wetting phenomena leads investigation of hierarchical surfaces which have surface structures in both micro and nano sizes. Wetting of hierarchical surfaces is illustrated in the Figure 1.4. Basically, four different wetting modes can be observed on the hierarchical surfaces. These modes can be expressed as

Wenzel state for both micro and nanosized grooves (Figure 1.4 (a)), Wenzel state for microsized cavities and Cassie-Baxter state for nanosized cavities (Figure 1.4 (b)), Cassie-Baxter state for micro sized cavities and Wenzel state for nanosized cavities (Figure 1.4 (c)) and Cassie-Baxter state for both micro and nanosized grooves (Figure 1.4 (d)).

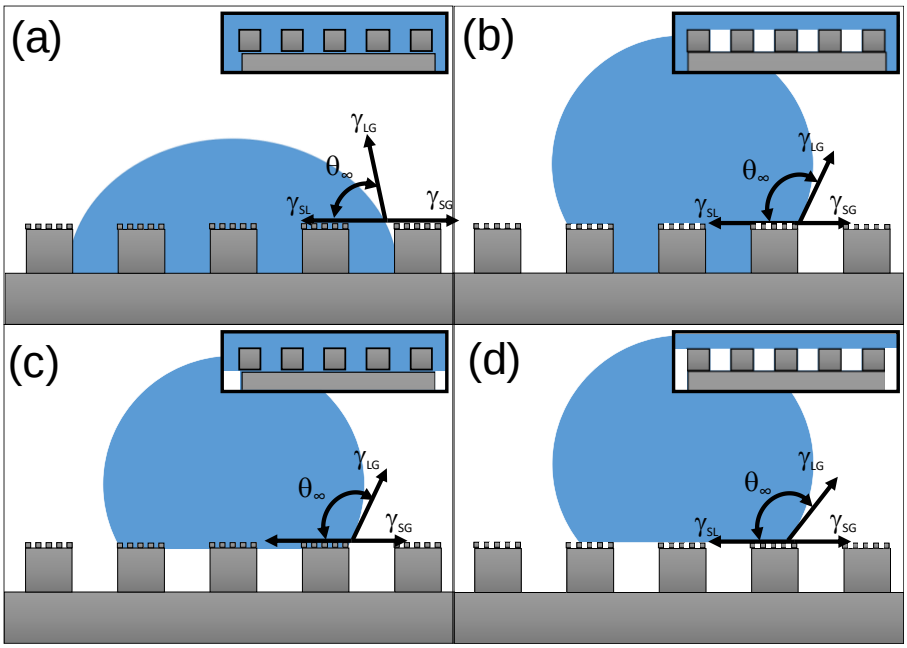

Figure 1.4. Wetting states of hierarchical Surfaces

1.2. Wetting in Nanoscale

As droplet size decreases, interfacial tensions are found to be insufficient in explaining wetting behavior of nanosized droplets because of size dependency which can change wetting dynamics in small size. A phenomenon called line tension results from tension appearing where the three phases (solid-liquid-vapor) meet should be considered in nanoscale wetting. Modified Young equation[17] is proposed to capture effect of line tension.

$$\gamma_{SG} = \gamma_{SL} + \gamma_{LG}\cos\theta_\infty + \frac{\tau}{r_B} \tag{1.7}$$

In equation 1.7, modified Young equation is presented and line tension is denoted with τ and r_B refers to base radius of droplet. As it can be clearly interpreted from equation 1.7, the effect of line tension is directly proportional with curvature of droplet which is reciprocal of contact line radius. Thus, for macroscopic droplets, line tensions become

negligible and as curvature of droplet ($1/r_B$) increases, the effect of line tension becomes significant, so line tension should be considered in nanoscale wetting.

The outline of this study can be organized as follows; In Chapter 2, basic aspects of molecular dynamics will be provided. In Chapter 3, molecular dynamics studies on wetting of smooth silica surfaces will be presented. In Chapter 4, molecular dynamics studies on wetting of nanopatterned silica surfaces will be presented and applicability of proposed models will be discussed. Finally, in Chapter 5, the study will be briefly covered and suitable conclusions will be made.

CHAPTER 2

MOLECULAR DYNAMICS SIMULATIONS

Molecular dynamics is a modeling of atomic or molecular motion in a system by employing Newton's laws. Each atom is modeled as a point mass and is subjected to force fields depending on quantum mechanical effects. In molecular dynamics, potential functions are required to model the force fields. Next, molecular forces exerted on each atom by the other atoms are calculated. Net force on atoms are extracted and are utilized to employ Newton's 2nd Law so that atomic tracjectories are found for a specified time interval.

In molecular dynamics, the first step is to specify atoms and their position in the system. Then, the domain of the system is introduced and generally, periodic boundary condition is employed because of infinitely small scales. Next, potential functions are defined in order to capture interatomic interactions. Lastly, the system is processed regarding ensembles and time integration is performed.

2.1. Potential Functions in Molecular Dynamics

Understanding phenomena and capturing characteristic of the system by employing physical laws and with minimum computation cost is essential in modeling. In molecular dynamics, potential should be determined carefully because a tremendeous number of potentials for atoms exists. Basically potential functions can be divided into two groups, pairwise and multi body potentials. Due to computational costs, pairwise potentials are generally desired, but many body potentials are required for systems that pairwise potentials are insufficient to model.

Lennard-Jones (L-J) potential is commonly used to model dispersive interactions between atoms. The distance in which potential becomes zero is important in L-J potential and it also called particle diameter. When the distance between atoms is smaller than the diameter, atoms repel each other and when the distance is longer than the diameter atoms attact each other. Since L-J potential has exponential 6 and 12 terms, it is named as a 6-12 potential.

$$E_{LJ} = 4\varepsilon\left[\left(\frac{\sigma}{r}\right)^{12} - \left(\frac{\sigma}{r}\right)^{6}\right] \quad (2.1)$$

L-J potential function is presented in equation 2.1. σ, ε and r terms denote atomic diameter, depth of a potential well and interatomic distance, respectively. When interatomic distance is smaller than the diameter, L-J potential function is valued positively and repulsive interaction between particle is observed. If the diameter is smaller than the interatomic distance, L-J potential results in negative values and attraction between particles is observed.

Electrostatic interactions are calculated in the system containing ions or molecules with electric charge. For some molecules, electrons attracted by the elements that higher proton number so polarization occurs. To model polarization, partial charges are assigned to elements of molecule. It should be noted that total net charge equals to zero even if polarization is observed. Therefore, sum of partial charges should be zero. Electrostatic interactions can be classified as short range and long range electrostatic interactions. Coulomb's law is employed to model short range of electrostatics interactions. Short range electrostatic interactions are generally calculated additively so L-J potential function can be modified with additional terms.

$$E_{LJ+Electrotatic} = 4\varepsilon\left[\left(\frac{\sigma}{r}\right)^{12} - \left(\frac{\sigma}{r}\right)^{6}\right] + \frac{q_i q_j}{\varepsilon r} \quad (2.2)$$

In equation 2.2, short range electrostatic interaction term added two L-J potential function is presented. q_i and q_j represent electric charge of two interacting particles and ε denotes dielectric constant. Additional correction terms can be added to equation 2.2 to increase computational accuracy.

Long range electrostatic potentials are much complex to implement and computationally expensive. There are two basic type of long range of electrostatic interaction functions which are PPPM (Particle Particle Particle Mesh) and Ewal Summation. PPPM method is implemented in this study because of its efficiency in computational time. In PPPM, initialy, maps charges in three dimensional domain and then Poisson equation on the meshes is solved by three dimensional fast fourier transform. Finally, electric field on the meshes is interpolated to find long range electrostatic interactions[18].

Complex potential functions, more complex than 2 body potentials, are required to model bulk structure of substrates and capture underlying physics of mechanisms. Many body potentials could be developed for specific atoms such as silicon potential

developed by Stillinger and Weber [19] or could be developed in certain form and parameters adjusted for different systems. For example, Tersoff potential is available for Si, SiC, SiCGe systems. Various attempts have been made to model bulk silica structure successfully. For example, van Beest *et al*. (BKS)[20] proposed ab inito based interatomic force field which consist of pairwise interaction between silicon and oxygen atoms. Similarly, another pairwise interactions based force field was developed by Pedone *et al*.[21]. The Tersoff potential, initially proposed for silicon structures, was modified by Munetoh *et al*.[22] to model silica structures. Moreover, Reactive force field (ReaxFFSiO) which allows to investigate chemical reaction was developed for silica by van Duin *et al*.[23].

2.2. Water Models

Due to the complex nature of water, various water models are proposed to capture physical properties of water using molecular dynamics. However, there is no model that can capture water properties inclusively. Therefore, water models should be chosen depending on the properties required to capture. In the literature, commonly employed water models are TIP3P[24] (Transferable Intermolecular Potential 3P), TIP4P[24] (Transferable Intermolecular Potential 4P), SPC[25] (Simple Point Charge), SPC/E[25] (Simple Point Charge Extended). To reproduce thermodynamically stable water models, short range dispersion forces, i.e. Lennard jones potential and electrostatic interactions are required, generally. Proposed models differ by diverse parameters such as L-J parameters of O and H atoms, partial charges assigned to O and H atoms, bond length and bond angle between O and H atoms. Moreover, to reduce computational cost, water molecules can be modeled as a rigid structure by fixing bond length between O and H atom.

2.3. Ensembles

In molecular dynamics, it is not feasible to model a system which has length scale greater that nanometer due to an excessive amount of computational burden so to reduce computational work and perform time efficient simulations, various methods are applied.

One of the most common methods is to fix the properties that are unrelated to study of interest and computational costs can be reduced. In order to achieve that ensembles of particles are formed. Therefore, ensembles are one of the musts in molecular dynamics simulation. Desired properties of particles are obtained using ensemble averaging technique which originated from the ergodic hypothesis. Basically, this theory assumes that when time dependent behavior of the particles is averaged long enough, extracted properties can be used as a substitute of macroscale behavior. To form ensemble, properties of systems like pressure, temperature, energy or etc are held fixed.

Common ensembles applied in MD are introduced as follows; if total particle number, total volume and total energy of the system or subsystem are kept constant, microcanonical (NVE) ensemble is formed. In microcanonical ensembles, heat transfer between system and environment is eliminated. Moreover, if total particle number, total volume and temperature of the system or subsystem are kept constant, microcanonical (NVT) ensemble is formed. Furthermore, when total particle number, total pressure and temperature of the system or subsystem are fixed, isothermal and isobaric (NPT) is employed. In both NVT and NPT ensembles to keep temperature fixed, heat baths are employed and among the others, Nose-Hoover heat bath, Berendsen heat bath and Anderson heat bath are applied commonly.

2.4. Time Integration Algorithms

In simulations, it is essential to assign initial conditions properly in order to not have a convergence problem. In MD simulations, initial conditions such as interactions between atoms and initial position of atoms are utilized to predict time dependent motion of atoms. Position of atoms are calculated in each time step and time dependent behavior of the system is obtained. To calculate the position of atoms in consequent time step, position, velocity and acceleration of particle are taken into account. At the beginning of the simulation, velocity of particles is assigned by applying Boltzmann distribution.

Efficient time integration algorithms are developed to capture time dependent characteristics of the system. Since Taylor series is frequently used to predict the value of a function at a specific point as function of its derivatives, time integration algorithms are generally developed with the help of Taylor expansion. When position function is denoted with r and its first time derivative, velocity function, can be expressed with v(t).

Acceleration, a(t), can be deduced as a time derivative of velocity function. In that context, t is assigned as a time and δt can be assigned as time step. Accordingly, Taylor expansion of position at the time t + δt, r(t + δt), is expressed as in the equation 2.3.

$$r(t + \delta t) = r(t) + \frac{v(t)}{1!}\delta t + \frac{a(t)}{2!}\delta t^2 \ldots. \quad (2.3)$$

Similarly, Taylor expansion of velocity at the time t + δt, v(t + δt) and accelaration at the time t + δt, a(t + δt) are shown in eqation 2.4 and 2.5 respectively.

$$v(t + \delta t) = v(t) + \frac{a(t)}{1!}\delta t + \frac{b(t)}{2!}\delta t^2 \ldots \quad (2.4)$$

$$a(t + \delta t) = a(t) + \frac{b(t)}{1!}\delta t + \frac{c(t)}{2!}\delta t^2 \ldots \quad (2.5)$$

Time integration algorithms used in MD simulations are generally obtained with the help of equation 2.3, 2.4 and 2.5.

2.5. Modelling of Water Droplet on Silica Surfaces

One of the main drawbacks in nanoscale wetting studies is size dependency which results from tension appearing where the three phases meet. Effect of line tension is related with contact line radius and as base radius of droplet decreases, effect of line tension becomes significant. As a result, droplets of various sizes are investigated in nanoscale wetting to distinguish the effect of size dependency. However, in MD simulations, semi cylindrical droplets are introduced to extinguish effect of line tension. In this method, semi cylindrical droplets are modeled rather than hemi-spherical ones and curvature of the three phase contact line is eliminated. With this method, wetting property of surface can be obtained regardless of nano droplet size. Therefore, semi cylindrical water droplets are formed during this study to minimize computational time and cost.

To model silica substrate multibody tersoff potential[22,47] is applied and SPC/E water model is choosen simulate water molecules. Molecular interaction parameters from literature are presented in Table 2.1. O-O and H-H parameters are obtained from SPC/E model of water and Si-O parameter is proven to be valid interaction parameter between silicon and oxygen atoms[36]. Potential parameters in the literature for oxygen atoms of water and oxygen from silica substrate are found to be questionable. Therefore, both ab initio and molecular dynamics simulation are performed to obtain these parameters and obtained parameters are discussed in the next chapter.

Table 2.1. Molecular interaction parameters used for SPC/E water model.

Molecule Pair	σ (Å)	ε (eV)	q (e)
O-O	3.166	0.006739	-0.8476
H-H	0	0	0.4238
Si-O[36]	2.633	0.01511	0

Contact angles are measured from time averaged mass density profiles. To obtain mass density profile, first NVT ensemble is employed to obtain system at desired temperature which is 300^0 K for this study. After 2 ns NVT ensemble, 2 ns NVE ensemble is applied. During NVE ensemble, the system is observed for any changes. After determining system is in equilibrium production runs are performed to obtain average mass density of water molecules. In Figure 2.1 a snapshot of simulation domain during production runs is presented.

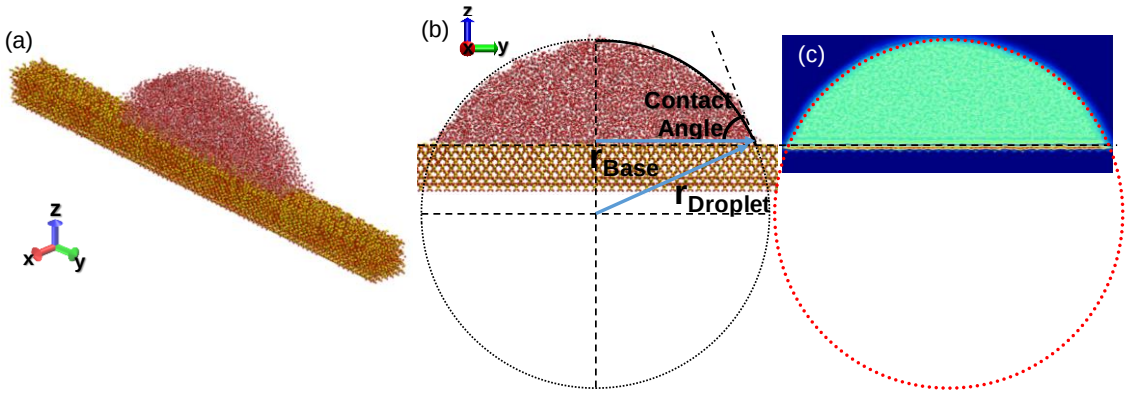

Figure 2.1. Measuring contact angles in MD studies (a) a snapshot from simulation domain (b) measurement of contact angle (c) water distribution

Water density is averaged into two dimensional pencil bins to extract water distribution in yz plane. In order to determine contact angle, initially, a circle encapsulating water droplet tangentially is introduced. Radius of the circle is stood for $r_{Droplet}$ in Figure 2.1(b). Also, r_{Base} is described to encircle contact region between water and solid substrate. Later, a line passes through three phase contact line and perpendicular to $r_{Droplet}$ is drawn. Contact angle of the droplet appears between the perpendicular line and r_{Base}. During this study, all contact angles are measured from water density distribution as shown in Figure 2.1(c) by measuring angle between r_{Base} and perpendicular line.

CHAPTER 3

WETTING OF SILICA SURFACES

Silica attracts the attention of wide variety of research areas such as drug delivery[26], colloidal[27] and environmental[28] sciences, micro-nanofluidics[29] devices and industrial processes[30]. Due to this vast interest, significant effort has been applied to model silica structures using computer simulations. Molecular dynamics (MD) is a state of the art method that is extensively employed to capture features of silica at the molecular level. However, success of MD simulation is strictly related to potential functions that are used to model interatomic potentials. Since silica is commonly exposed to aqueous environments, force fields of water-silica systems are introduced for various applications. Interaction between water and α-quartz surface was studied by Lopes *et al.*[31] after optimization of CHARMM force field parameters to model pathogenic processes caused by silica. Additionally, CHARMM force field was developed for amorphous silica by Cruz-Chu *et al.*[32] and water behavior in silica nanopore was studied. Furthermore, to investigate water silica interface previously developed force fields for silica were modified. For instance, with the help of ab initio studies, BKS potential was extended by Hassanali and Singer[33] to model amorphous silica-water interfaces also ReaxFFSiO is modified to investigate chemical activities of the interface in detail by Fogarty *et al.*[34].

Wetting is one of the most fundamental concepts originating from interfacial phenomena so contact angle plays an important role in surface characterization[6]. Also, surface engineering by adjusting wetting to obtain anti-ice or self-cleaning is employed commonly. For example, wetting and boiling of a silica surface which is engineered and structured with self-assembled monolayers showed that as wetting increases, boiling heat transfer increases so high heat transfer performance can be obtained[4]. Aditionally, by tuning wetting to super hydrophobicity, bactericidal behavior can appear on the surfaces and designing such anti-bacterial surfaces could be required for microfluidics, medical instruments and anti-biofouling applications[35]. For this reason, modeling wetting properties of materials such as silica is highly desired due to vast number of interfacial phenomena related applications. Wetting is simply equilibrium condition between adhesion and cohesion forces and to model wetting in MD, non-bonded interactions

between water molecules and solid substrate are required to capture. The simplest force field form, which is pairwise potential, is enough to reproduce wetting and basics of interfacial phenomena. However, in order to model wetting of silica substrate, force fields are either too complex, expensive due to computational costs, or only valid for ad hoc cases. Therefore, transferable and computational cost friendly force field could ease wetting related studies of silica and help to broaden understanding of wetting for new applications.

Lennard-Jones (L-J) potential is one of the most commonly used pairwise potential to express interatomic non-bonded, Van der Waals interactions and consists atom specific constants such as depth of a potential well (ε) and the distance where inter-particle interactions are zero (σ). The problem arises when L-J potential is applied to model interactions between different kinds of atoms because empirical method, known as mixing rule, is employed to derive interaction parameters. Lorentz-Berthelot (L-B) mixing rule is basically obtaining arithmetic and geometric mean of σ and ε parameters, respectively, to define interaction constants but it is presented that L-B mixing rule fails in capturing wetting behavior of silicon surface because interaction parameter between oxygen and silicon atoms overestimated [36]. Therefore, it should be underlined that due to lack of underlying physics, L-B mixing rule could fail. Moreover, interaction parameters suffer from transferability due to the mixing rule. For example, since parameters are suggested to reproduce silica structure, when force field of silica is changed, interaction parameters so interaction characteristics between water and silica are changed. As a result, silica force field specific studies are conducted and transferable interaction parameters, regardless of force fields, between silica and water is missing in the literature.

Silica is known to be hydrophilic but experimental wetting angles of silica vary between 7^0 and 92^0 degrees and huge variation is attributed to insufficient surface treatment surface contamination in silica substrates[37]. In the Figure 3.1, contact angle of semi cylindrical water droplet containing 1280 water molecules on silica surface by using L-J parameters from Table 2.1 is presented. Since there are no specific transferable parameters to model the interaction between oxygen atoms of silica and water molecules, oxygen parameters of SPC/E model are employed but using parameters results in poor contact angle prediction. Existing interaction parameters overestimate wetting angle of water droplet and fail in capturing hydrophilic nature of silica surfaces. Furthermore, poor prediction of contact angle is expected because electron configuration of oxygen atoms in water molecules is different than oxygen atoms in silica. Therefore, assigning identical

interaction parameters for different kind of oxygen atoms is irrational but according to our knowledge, there is no transferable interaction parameters between oxygen atoms of two different kind are proposed to capture wetting of silica. Thus, it is considered that these interaction parameters should be visited first to capture wetting characteristic of silica surfaces. To solve this, studies should be conducted to find transferable interaction parameters between water-silica.

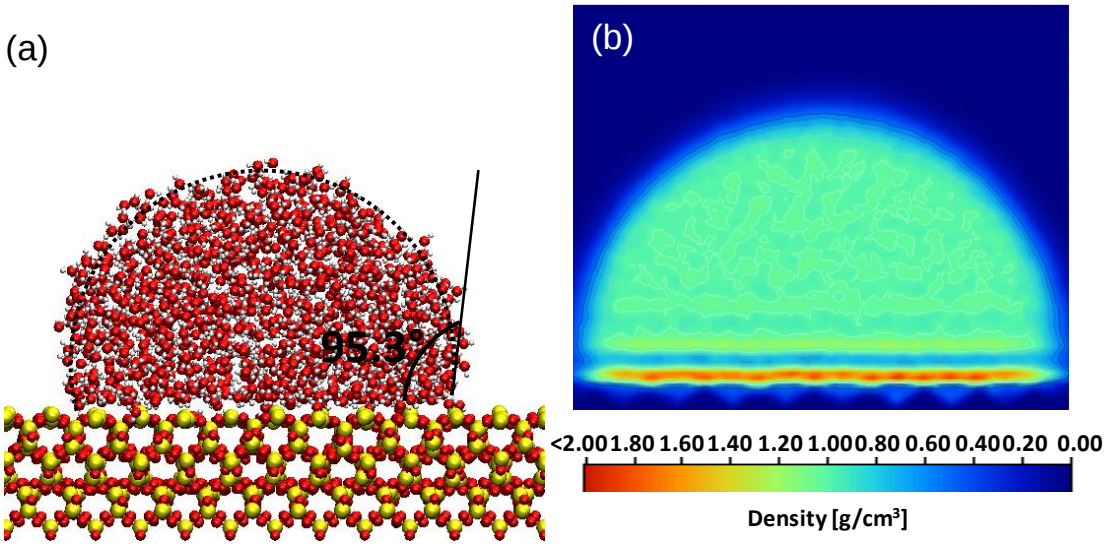

Figure 3.1. Wetting study with standard force field parameters on smooth silica surface (a) snapshot from MD simulation (b) water density distribution of droplet

According to our knowledge, two different methodologies to find transferable interaction parameters exist. The first method performs a parametric molecular dynamics study as proposed by Werder *et al*.[38] to model graphite water interaction and the method is based on variation of interaction strength between oxygen and carbon atom to reproduce wetting on graphite. Similar studies are performed for water-silicon and water-silicon carbide systems. Although it is claimed by Cruz-Chu and *et al*. that CHARMM force field based [32] which was developed depending on contact angle measurement and the same method was followed in their study, due to mixing rule proposed parameters were prone to silica force field. Hence, there is a gap in the literature about transferable force field to describe wetting of silica. The second method to investigatewetting characteristics of surfaces is to perform first principle calculations to obtain accurate non bonded interaction parameters. Past studies show that ab initio simulations provide results consistent with the experimental ones. Heiranian *et al*.[39] performed this computational modeling tool to get accurate force field parameters of MoS2-water interface. Besides

that, Wu *et al*.[40] also carried out first principles quantum Monte Carlo simulations to determine non bonded interaction parameters between hBN and water.

In this chapter, in order to develop transferable L-J force field between silica and water two different methodologies are followed. First, Ab initio based calculations are employed and ab-initio based force field is proposed for silica-water system. Then, molecular dynamics simulations are performed to investigate interaction strength between amorphous silica and water molecules. In both cases, developed force field are compared with experimental contact angle measurements on silica surfaces.

3.1. Developing Ab-initio Based Force Field for Silica Wetting

Since ab initio calculations allow us to obtain potential energy surface, calculated interaction energies help developing force fields for molecular dynamics simulation. Therefore, to understand wetting behavior of silica surface, first principle calculations are employed first. Alpha quartz polymorph of silica is chosen to silica structure because of themodynamically stable structure at low temperatures. Before calculations, adsorption of single water molecule is investigated to specify the location where indentation of water molecule is performed After selecting possible adsorption sites which are shown in Figure 3.2, indentation is performed. Although it is unlikely to assume site-4 as a possible adsorbtion site, it is examined to understand behavior of water molecule under weak interactions. Before the indentation, water molecule is located at least 7 Å away from the top layer of silica structure. Then, the water molecule approaches the surface vertically. At every distance, potential energy of the system is investigated to obtain potential energy curves and during these steps, oxygen of water molecule is constrained but hydrogens of water molecule is allowed to move freely to obtain minimum energy of the system.

Before the indentation, silica structure is relaxed to obtain minimum energy configuration of the system. Potential energy curves of each site and binding energies are presented in Figure 3.3. It can be observed that each site has different binding energy and site 1 and site 4 have lower binding energies than the other sites. Therefore, it can be inferred that site 2 and site 3 are more favorable than the other site so strong binding energies are obtained from these sites. That's why, to model non-bonded interactions, site 1 and site 4 are desired because strong binding energy.

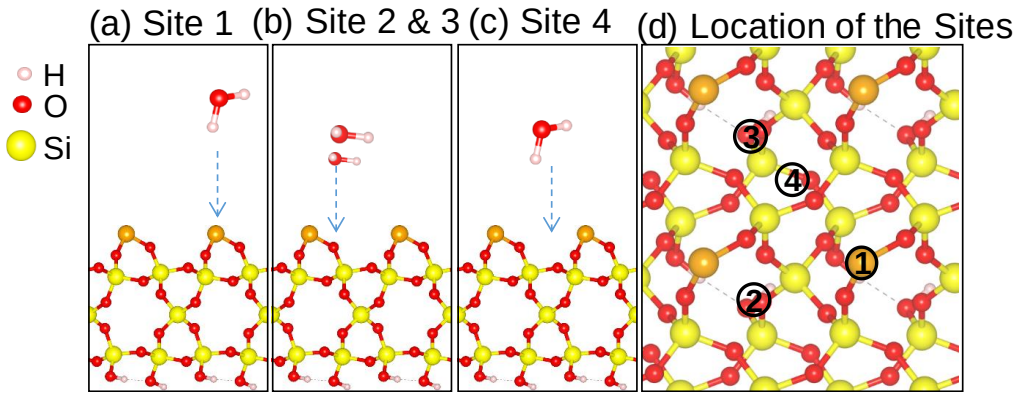

Figure 3.2. Location of sites to obtain potential energy curves of silica surface (a), (b), (c) are side views of site 1, site 2 & 3, site 4, respectively, on the silica structure. Indentation process of single water molecule to site1 and site 4 is represented (d) Top view of [100] silica surface and location of sites. Orange atoms represent the topmost silicon atoms.

Interaction energy between water molecule and silica surface is extracted by subtracting energies of water molecule and silica structure from total energy of systems. Then, obtained potential energy curves are assumed to be in the form of L-J function since dispersive interaction of H atoms are negligible small so the fit equation to express interaction energy is expressed as follows

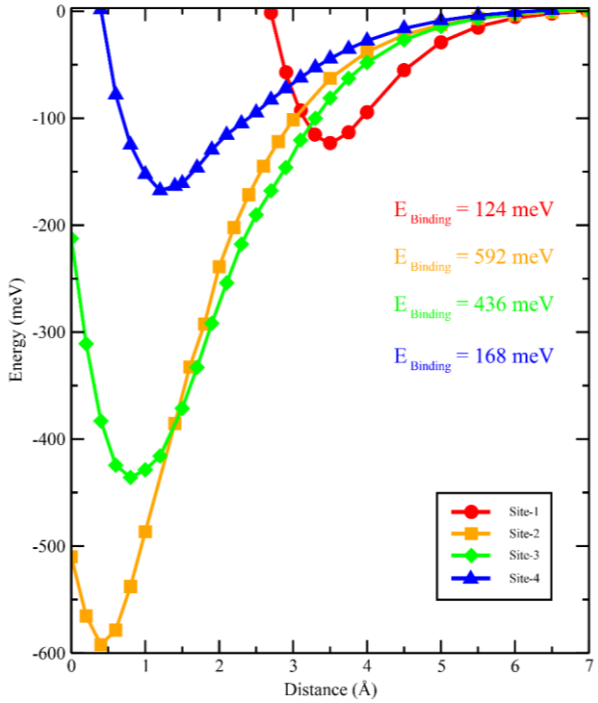

Figure 3.3. Potential energy curves of different sites on 100 α-quartz surface as a function of distance and binding energies of the sites.

$$\Delta E = \sum_{i \in Si} 4\varepsilon_{Si-Ow}\left(\left(\frac{\sigma_{Si-Ow}}{r_{i-Ow}}\right)^{12} - \left(\frac{\sigma_{Si-Ow}}{r_{i-Ow}}\right)^{6}\right) + \sum_{i \in O} 4\varepsilon_{O-Ow}\left(\left(\frac{\sigma_{O-Ow}}{r_{i-Ow}}\right)^{12} - \left(\frac{\sigma_{O-Ow}}{r_{i-Ow}}\right)^{6}\right) \quad (3.1)$$

Where subscript of *Si*, *O* and O_w denotes silicon atoms, oxygen atoms in silica and oxygen atom of water molecule, respectively. Equation 3.1 clearly shows that four parameters are required to capture interaction energy, but further assumptions could be made to develop a force field that is applicable for both silicon and silica surfaces. By that reason, interaction parameters between silicon and oxygen of water are accumulated from the literature which successfully reproduces wetting of a silicon structures and interaction parameters between oxygen of water and oxygen of silicon atoms can be obtained by fitting potential energy curves.

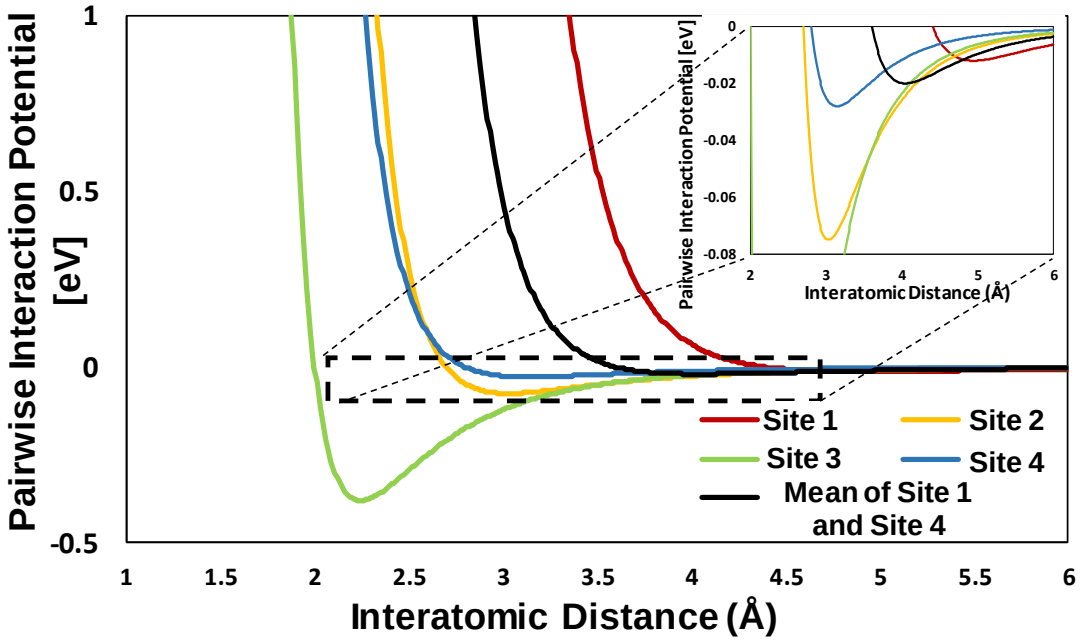

Figure 3.4. Potential energy between dissimilar oxygen atoms as a function of distance

For every site of silica surface, fitting is performed and fit parameters are presented in the Table 3.1. In Figure 3.4, pairwise potential-distance curves of presented parameters are provided. It can be inferred from both Figure 3.4 and Table 3.1 that lower interaction strengths are observed on the sites which have reasonable binding energies to capture non-bonded interactions. Maximum interaction strength is extracted from Site 3 although maximum binding energy is obtained from Site 2. Therefore, it should be noted that aim of fitting is to capture behavior of potential energy curves and extracted

interaction parameters express interaction between dissimilar oxygen atoms which are part of silica structure and water molecule. Since binding energy depends on local electron density but due to additive pairwise potentials, interaction strength is affected by orientation of atoms and distance between pairs. Thus, sites that have maximum binding energy and sites that maximum interaction strength could mismatch. Furthermore, lowest interaction strength is obtained from Site 1. Even though Site 2 results in similar interaction strength with site 4, it is not considered to model wetting study due to high binding energy. Similarly, Site 3 excessively overestimates interaction strength. Therefore, both binding energies and fit parameters suggest considering Site 1 and Site 4 to model force field and final wetting parameters are utilized as a mean of Site 1 and Site 4 to perform molecular studies.

Table 3.1. Molecular interaction parameters fitted for O-O_w water model

Site	σ (Å)	ε (eV)
1	4.4	0.012
2	2.7	0.075
3	2	0.38
4	2.8	0.028

Representative measurement of contact angle is shown in Figure 3.5 (a). To measure contact angle, density contours are obtained from averaged water density profiles and then circular segment is fitted to density contours. Depending on base radius and droplet radius ($r_{Droplet}$) of circular segment contact angle is measured. Contact angle is measured 9.340 from averaged water density distribution as presented in Figure 3.5 (b). Furthermore, it can be inferred from Figure 3.5 (b) that near interface density shows that strong layering of water molecules and density of that region exceeds double of expected water density, that's why density profile in strongly layered region is neglected during contact angle measurements.

Experimental studies about wetting of silica suggest wide range of contact angle such as from 7^0 to 92^0 degrees on the surface[37]. The main reason of the inconsistency is surface contamination or surface cleanliness and depending on surface cleaning method,

contact angle of the surface can vary[37]. Although contact angle of silica surfaces is in the range of experimental studies further force parametrization is needed because Ramos-Alvarado *et al.*[41] mentions ab inito based potentials underestimates contact angles in wetting studies and due to variety in binding energies, empiric parametrization of interaction potentials should be applied. Therefore, in order to obtain force fields parameters, interaction strength is tuned to yield in experimental contact angles of silica.

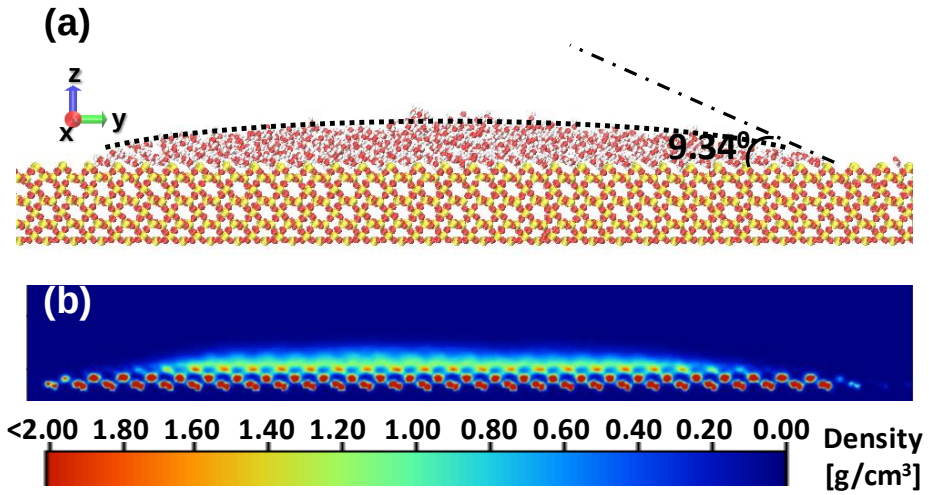

Figure 3.5. (a) Representative measurement of contact angle from hemispherical droplet. Silicon, oxygen and hydrogen atoms presented in yellow, red and white, respectively. (b) Averaged of density distribution of water molecules.

3.2. Tuning Interaction Strength for Silica Wetting

β–cristobalite form of silica is used as a silica structure during this study because density of beta cristobalite is similar to amorphous silica so it can be used as a substitute of amorphous silica, which is commonly used in MD studies because of the crystal structure[42,43]. Therefore, contact angle of non patterned beta cristobalite surface is assumed analogous to contact angle of amorphous silica structures. A recent study shows[44] that contact angle of amorphous silica is approximately 55^0 when there is no surface processing is performed. In another study[45], wetting angle of silica surface is presented as 48.4±0.9. Moreover, wetting angle of silica is proposed approximately 40^0 by others[32,46] so it can be said that ab initio based calculations overestimates interaction parameters.

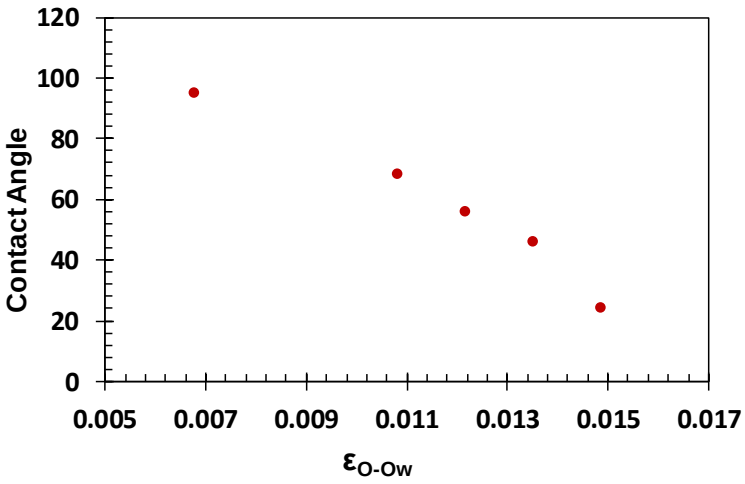

Figure 3.6. Contact angle of silica as a function of epsilon parameter

Systematical MD simulations are performed on smooth silica surface by altering interaction strength between oxygen of water and oxygen of silica. Interaction strength between silicon and oxygen atoms of water molecules is extracted from the literature[36] to assure valid force fields for both silica and silicon surfaces. SPC/E water model is employed to model water droplet which consist of 1280 water molecules. In Figure 3.6 variation of contact angles as a function of interaction strength between oxygen of water and oxygen from silica ($\varepsilon_{O\text{-}Ow}$) is presented. It is found that for 0.0121 eV and 0.0135 eV values of $\varepsilon_{O\text{-}Ow}$ parameter, wetting angles of silica are measured with 56^0 and 46.2^0. These contact angle values are in good agreement with experimental contact angles which are 55^0 and 48.4^0. Therefore, these interaction parameters are acceptable to use in modeling wetting on nanopatterned surfaces. Moreover, these parameters correspond to $1.8*\varepsilon_o$ and $2.0*\varepsilon_o$ where ε_o refers to interaction parameter between oxygen atoms in SPC/E model of water.

Although, it is mentioned that in MD studies cylindrical droplets are used to obtain size independent contact angle measurements, we aim to ensure validity of the proposed force field parameters so further MD simulations are performed to question size independency of cylindrical droplets. In that purpose, four different droplet volumes are chosen to investigate wetting behavior on a smooth silica surface. Water droplets which have 1200, 3000, 5000 and 8000 water molecules are modelled. Wetting behavior of both cases are investigated and contact angle measurements of water-silica systems are shown in Figure 3.7, whichshows that negligible changes are observed as the size of the droplet changes. Small changes could originate from thermal fluctuations. Therefore, it can be

inferred from the Figure 3.7 that cylindrical droplets in MD wetting studies lead size independent contact angle measurements.

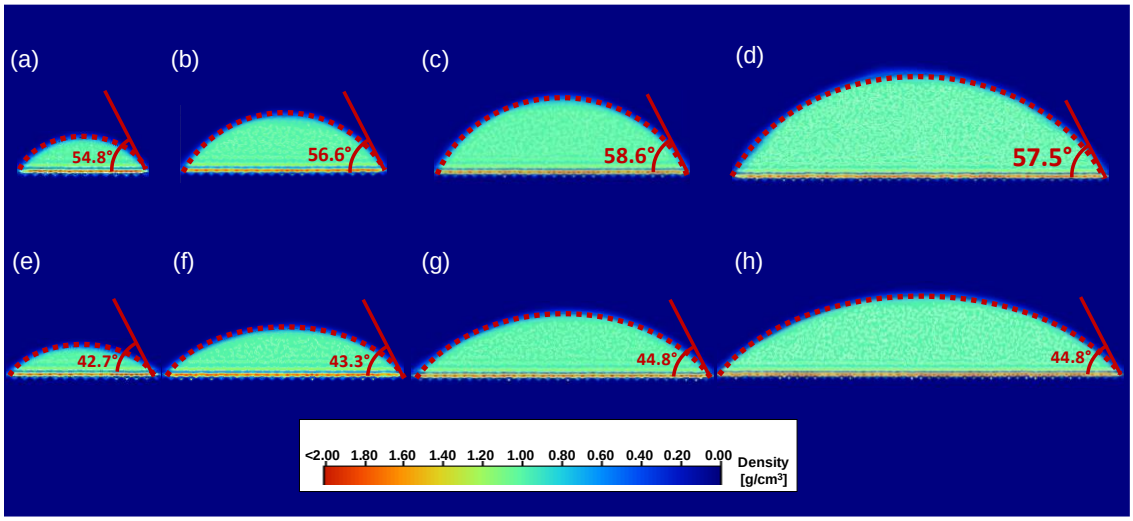

Figure 3.7. Investigation of size independency of cylindrical water droplets. (a), (b) , (c) and (d) shows wetting angle of droplets with 1200, 3000, 5000 and 8000 water molecules, respectively for 1.8*εo case. Similary, (e), (f), (g), and (h) shows wetting angle of droplets with 1200, 3000, 5000 and 8000 water molecules, respectively for 2.0*εo case.

Using the proposed interaction parameters, wetting of water-silica systems can be modeled with simple L-J parameters and computational costs of the simulations are reduced. Moreover, interaction parameters suffer from transferability due to the mixing rule being no longer needed. Therefore, wetting behavior of silica surfaces can be reproduced regardless of potential functions to model silica substrate. With these parameters silica-water interface is preserved even if force field of silica is changed. Thus, proposed parameters are applicable for every MD simulation on wetting of silica surfaces.

CHAPTER 4

WETTING OF NANOPATTERNED SILICA SURFACES

Wetting on nano sized rough surfaces has attracted a great amount of attention to understand wetting mechanism. Efforts have been made to correlate the effect of nano scale roughness to macroscopic theories such as Wenzeland other experiemental studies[48–50] support applicability of Wenzel model for the length scales greater than 100 nm on rough surfaces. Moreover, Wenzel model is found to be more appropriate than Cassie-Baxter model in nanoscale but deviation between Wenzel model and measured contact angle is observed[51]. Similarly, it is asserted that Wenzel model is valid for cavity width longer than 8 nm[52]. On the other hand, on molecularly rough surfaces, disagreement with the Wenzel model is observed[53]. Therefore, no concensus is established on wetting behavior of surfaces with nanosized structures.

Efforts have been made to combine two different wetting models to explain wetting behavior of patterned surfaces. First, combined model is aimed to explain wetting angle as a function of invading distance which measures depth of a fluid penetrating into cavity[54]. Later, Marmur[55] is proposed to investigate wetting behavior of partially wetted cavities by considering partially wetted area. Moreover, a model is proposed for a surface which liquid film invades cavities[56]. However, these models are in conjuction with macroscopic models. Recently, a model was proposed to predict hybrid Cassie-Baxter and Wenzel models for both hydrophilic and hydrophobic surfaces in nanoscale[54]. Furthermore, empirical model considering Wenzel and Cassie -Baxter angles as limits of possible contact angle is proposed[57].

In this chapter, wetting on nanopatterned silica surface is investigated to develop a general understanding on the effect of nanoscale roughness. Hypothetically, two different silica structures with two different contact angles are used. For both structures, contact angles are measured on ten different nanopatterns. To make a distinction between cases, silica structures are specified as case 1 and case 2. Case 1 denotes hydrophilic contact angle which is 56^0 and case 2 means more hydrophilic case which has contact angle 46.2^0 Wetting behavior on corrugated surfaces are compared with macroscopic

wetting models such as Cassie-Baxter and Wenzel. Also, hybrid approach is followed to characterize wetting behavior.

4.1. Nanopatterned Silica Surfaces

β–cristobalite form of silica structure is advantageous because of its crystal structure. As a part of its nature, β–cristobalite forms honeycomb structures and develops roughness patterns. If repeating honeycomb structure is assumed to be unit roughness element, then roughness patterns are denoted as Rxyz where x stands for the number of unit roughness element on the pattern, y denotes the number of removed unit roughness element in the pattern and z is the number of vertical O-Si-O layer which is removed. In this analogy, roughness patterns are shown in Figure 4.1.

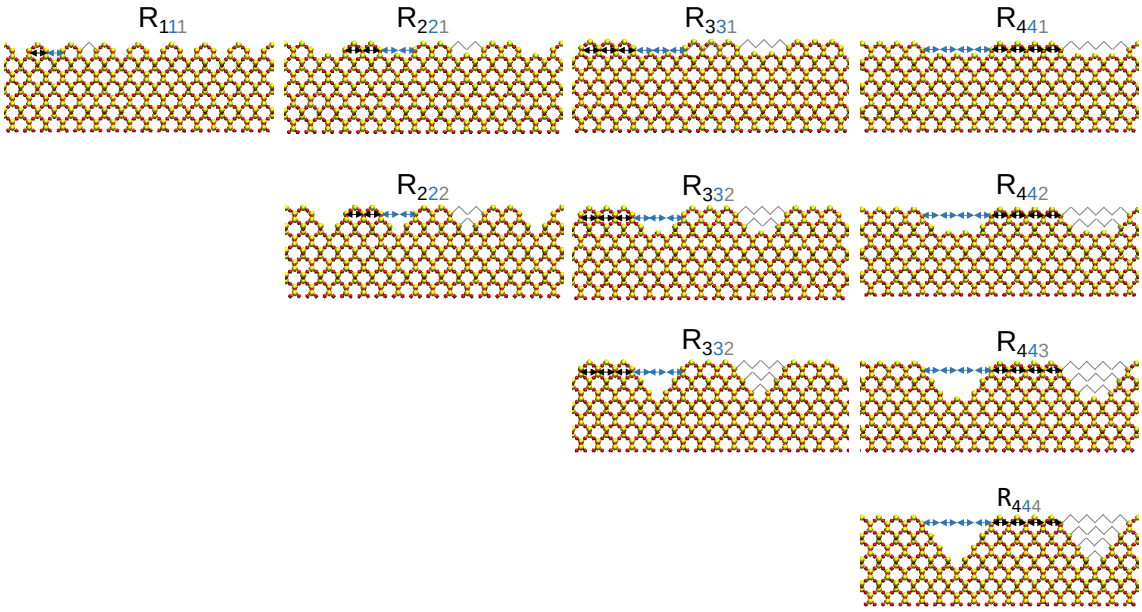

Figure 4.1. Nanopatterned silica surfaces

4.2. Wetting of Nanopatterned Silica Surfaces

Simulation domain is formed by a silica slab and a nano-scale water droplet. Simulation box is formed approximately 30m×4nm×20nm dimensions in x×y×z-directions, correspondingly. Periodic boundary condition is imposed on x and y direction while z-direction was bounded with a reflective boundary which flips velocity of particles

to keep particles inside the simulation box. Contact angle of droplets are measured from time averaged water densities. Water density is averaged in pencil bins with size of 0.5×0.25 A to obtain water distribution in yz plane. NVT ensemble is first employed to allow the system to reach equiliblium. Then 2 ns NVE ensemble is applied and the system is observed for any changes. After assuring that system is in equilibrium, production runs are performed to average density of water moleucles for 2 ns. Density contours are extracted from areal water distribution and droplet shapes.

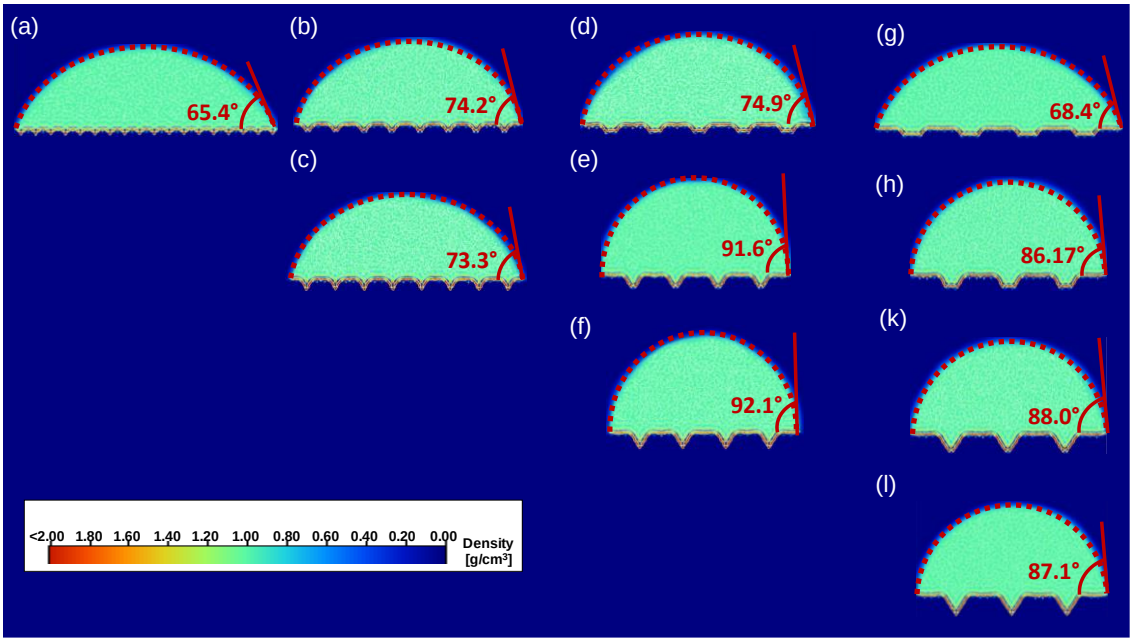

Figure 4.2. Contact angles of case 1.

Contact angles of case 1 presented in the Figure 4.2. Contact angles increase for each corrugated surface. In case 1, lowest contact angle is observed on the surface which has minimum pattern depth and width but for maximum cavity width and same cavity depth contact angle is very similar. When width of cavity is approximately 1 nm, Figure 4.2 (b) and (c), depth of cavity has no significant influence on wetting, for both cases contact angles are almost identical. However, for higher cavity width, i.e. Figure 4.2 (g), (h), (k) and (l), an increase in the cavity depth initialy leads to increase in contact angle but after one layer depth effect of cavity depth stays fixed. A similar trend is also observed for another cavity width on Figure 4.2 (d), (e) and (f). Furthermore, hydrophobic wetting behavior is observed on R_{332} and R_{333} surfaces.

Contact angles of case 2 are presented in Figure 4.3. Similar to case 1, all of the contact angles on corrugated surfaces are higher than smooth surface. Maximum contact angle is observed on R_{222} surface and minimum contact angle is observed on the surface

that has maximum cavity width and 1-layer depth. Similar to case 1, the effect of cavity depth disappears for R_{333}, R_{443} and R_{444} surfaces when the depth of cavity is larger than 1 layer. Unlike case 1, no hydrophobic wetting behavior is observed on any of the corrugated surfaces.

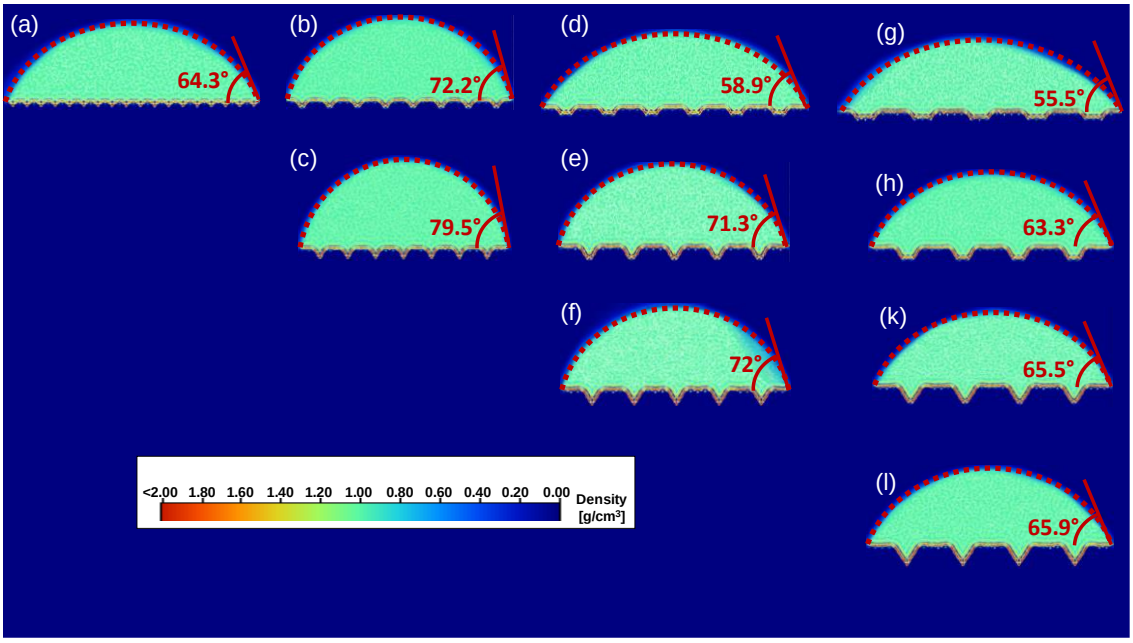

Figure 4.3. Contact angles of case 2

So far, investigated surfaces have homogeneously distributed cavity width and pillar width. However, those surface structures are insufficient to provide effect of pillar width on wetting. Therefore, further wetting studies are performed on different surface structures. Moreover, three different new surface structures are designed to investigate effect of pillar width. Designed surfaces are similar to R_{331}, R_{332} and R_{333} surfaces by the means of cavity width and cavity dept but pillar width of new surfaces is lessened, and one roughness element is kept as a pillar. Therefore, new surfaces are denoted as R_{131}, R_{132} and R_{133}.

In Figure 4.4 (a), designed R_{131}, R_{132} and R_{133} surfaces are shown. It can be obtained from the Figure 4.10, that wetting angles of R_{131}, R_{132} and R_{133} surfaces for case 1 are 74.0^0, 95.2^0, and 95.7^0, respectively. Similarly, wetting angles of R_{131}, R_{132} and R_{133} surfaces for case 2 are 62.0^0, 82.5^0, and 82.8^0, respectively. Moreover, there is no significant effect of cavity depth after one layer which is observed for both cases. Wetting angles of R_{132} and R_{133} surfaces are similar. In order to understand effect of pillar width, wetting angles of R_{131}-R_{331}, R_{132}-R_{332} and R_{133}-R_{333} surfaces should be compared individually because of the same cavity volumes. In that sense, for case 1, no convincing

effect of pillar width is observed because wetting angle of R_{131}, R_{132} and R_{133} surfaces are quite similar to R_{331}, R_{332} and R_{333}, respectively. On the other hand, for case 2, wetting angle significantly increases when pillar width decreases. Contact angles of R_{132} and R_{133} surfaces are approximately 10^0 higher than R_{332} and R_{333} surfaces. Therefore, it can be said that pillar width is an important parameter in wetting behavior of rough surfaces and pillar width should be considered to characterize wetting behavior.

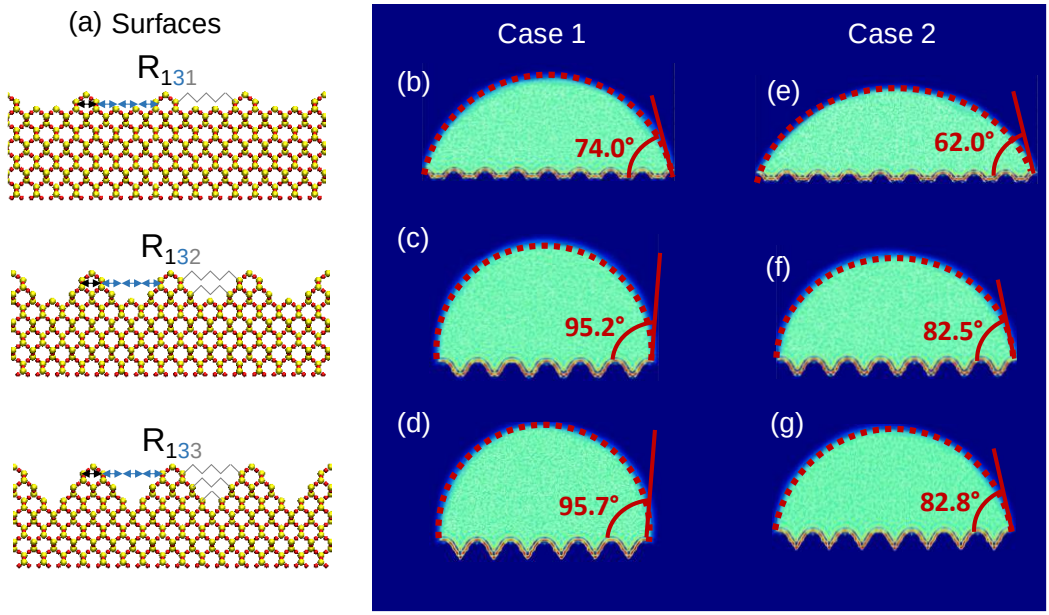

Figure 4.4. Wetting angles of R_{131}, R_{132} and R_{133} surfaces for case 1 are (b), (c), and (d), respectively. Similarly, wetting angles of R_{131}, R_{132} and R_{133} surfaces for case 2 are shown in (e), (f) and (g), respectively.

4.3. Wetting Angle Prediction of Wenzel and C-B Models

C-B and Wenzel models are based on the assumption that surface interfacial tensions are linearly proportional with interfacial areas. Both models consider effect of roughness in a straightforward correlation. For example, roughness ratio r defines ratio of actual area to projected ratio and Wenzel model assumes that solid-liquid interfacial tension increase proportional with roughness ratio, r. Similary, C-B model assumes interfacial tensions linearly change as a function of surface fraction, f. Both f and r parameters are calculated depending on size and shape of surface structures and in Table 4.1 roughness parameters of corrugated surfaces used in this study are presented. Roughness ratio of R_{111}, R_{222} and R_{444} surfaces yield in same value. Also, roughness ratio

of R_{221} and R_{442} surfaces are identical. Since number honeycomb structures removed from the surface and kept on the interface are the same for most of structured surfaces, surface fraction, f, of surfaces results in the same value except from R_{133} surface. It should be noted that topmost part of honeycomb structure has two inclined surfaces so surface fraction of the symmetrically patterned surfaces differ than 0.5.

Table 4.1. Roughness parameters of patterned surfaces

	Roughness Ratio-r	Surface Fraction-f
R_{111}	1.289	0.612
R_{131}	1.144	0.306
R_{132}	1.289	0.306
R_{133}	1.433	0.306
R_{221}	1.144	0.612
R_{222}	1.289	0.612
R_{331}	1.096	0.612
R_{332}	1.192	0.612
R_{333}	1.289	0.612
R_{441}	1.072	0.612
R_{442}	1.144	0.612
R_{443}	1.217	0.612
R_{444}	1.289	0.612

Applicability of macroscopic model on nanoscale roughness is investigated in Figure 4.5. It can be noted that Wenzel model underestimates contact angle of the surfaces. According to Wenzel model, when surface is hydrophilic(hydrophobic) roughness makes the surface more hydrophilic(hydrophobic) or vice versa so observed behavior in contact angles contradicts with Wenzel model because roughness increases contact angle while Wenzel state is observed. On the other hand, C-B models mostly overestimate contact angle but for R_{332}, and R_{333} surfaces of case 1, C-B model is in agreement with nanopatterned rough surface. However, for case 2, wetting angles of same surfaces are overestimated by the same model. The reason of the disagreement between macroscopic models can be originated from mean field approximation. Therefore, local effects such as density layering inside the grooves or pinning near the pattern edges[51], might be the reason for deviation from macroscopic models. For this reason, macrospic

models are found to be insufficient for wetting angle characterization of nano patterned surfaces.

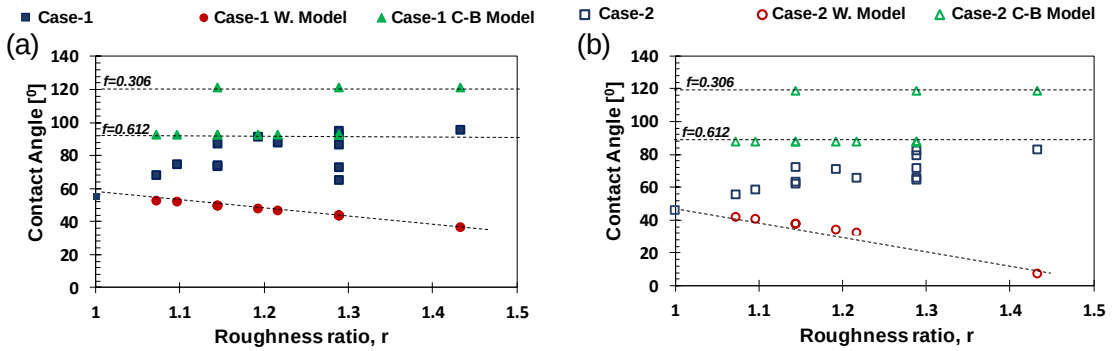

Figure 4.5. Contact angle prediction of Wenzel and Cassie-Baxter models and measured contact angles of nanopatterned silica (a) Case 1 and (b) Case 2

4.4. Effect of Water Density on Wetting Angle

Another approach to predict contact angle is to integrate water density with interaction potential to find solid-liquid interaction energy per unit area. Within this approach, complex body problems are handled as an approximate single particle average to reduce complexity. Mean field approach is generally employed to calculate wetting angle of a substrate analytically and wetting of smooth silicon[41], graphite[41] and silicon carbide[58] surfaces is predicted successfully by using mean field approach. In mean field approach, work of adhesion, W_a, is calculated analytically considering interaction potentials and water density distribution. Then, contact angle is extracted from work of adhesion. Describing water density at the interface is crucial to predict the contact angle because first layer of liquid near the density is directly related with wetting angle of the surface in mean field approach.

$$W_a = \gamma_{LG}(1+\cos\theta_\infty) \tag{4.1}$$

Since water density near interface is correlated with wetting angle, near interface densities of both cases is investigated. To make a comprehensive study, water density is investigated both locally and throughout the the pattern. Local investigation is performed by dividing roughness pattern into two. Near interface density profile on top of the pattern and inside the pattern cavity is extracted separately. Extracted local bin densities are first aligned such that density peaks along z direction shifted to same height and then density

profiles are averaged along y direction. Schematical illustration of near interface densities is shown in Figure 4.6.

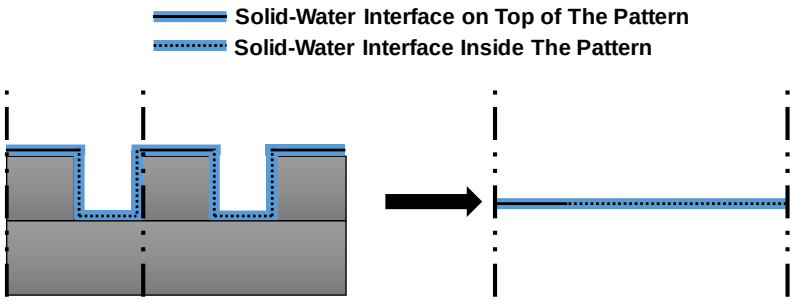

Figure 4.6. Representation of near interface densities on top of the pillar and inside the cavity

Obtained averaged densities for both cases are presented in Figure 4.7. Figure 4.7 (a), (c) and (e) are densities of top of the pattern, inside the pattern and averaged density along whole pattern, repectively, for case 1. Similarly, Figure 4.7 (b), (d) and (f) are densities of top of the pattern, inside the pattern and averaged density along whole pattern which is both inside the cavity and on top of the pattern, for case 2, respectively. When near interface density on top of the pattern is investigated for both cases, no agreement is observed. R_{111} surface of case has maximum density layering on top of the pattern but R_{221}, R_{442} and R_{444} surface of case 2 have maximum density layering which is almost identical. It is interesting to see that since case 2 has higher interaction strength, it is expected highest density layering will be observed on case 2. However, case 1 has approximately 10% more density layering on the surface which has maximum density layering. When density in the pattern cavity is investigated, highest density layering appears on R_{443} surface of case 2 but for case 1, maximum layering is observed on R_{222} surface. Again, no agreement between the two cases is observed. Average density through the pattern, highest density layering is seen on R_{444} surface of case 2 and maximum density of case 1 is monitored on the same surface. However, when wetting angles of these surfaces are considered, highest wetting angle is measured on R_{333} surface for case 1 and R_{222} surface for case 2. Furthermore, minimum contact angles are measured on R_{111} of case 1 and the same surface has maximum density layering on top of the pattern and minimum density layering inside the cavity but, there is no similar relation for other counterpart. Although, some links have been found between density layering and contact angle, no comprehensive link has been established. That's why it can be deduced that

mean field base theories are insufficient to predict contact angle of nanopatterned surface because of contradictory behavior in water density profiles.

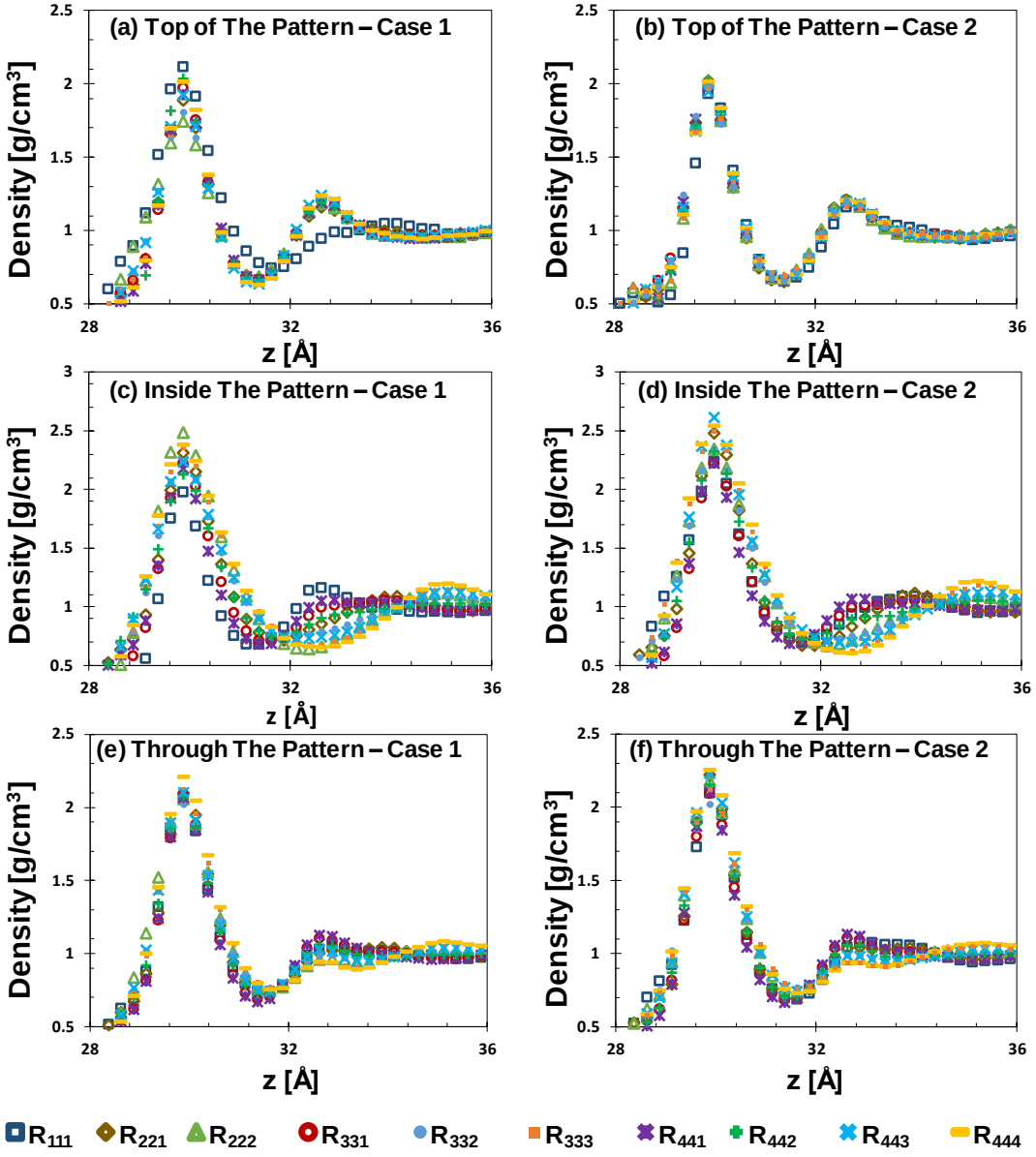

Figure 4.7. Near interface densities of patterned surfaces

4.5. Hybrid Cassie-Baxter and Wenzel Model

Among the other hybrid Cassie-Baxter and Wenzel models, the one proposed by Yen and Soong[54], seemed to be appropriate for case 1 and case 2. Their approach considers both roughness and geometrical parameters of patterns and liquid density inside the cavities. Briefly, an approximation is offered to distinguish Wenzel state and Cassie-

Baxter state depending on average density normalized with bulk density inside the cavity. They assumed that when Wenzel state is fully applicable, average density inside the cavity should be equal to bulk density. Therefore, deviation from bulk density inside the cavity originates from the presence of both Cassie-Baxter state and Wenzel state. Their model is presented as follows:

$$\cos\theta_{C-W} = f_W \cos\theta_W + (1 - f_W)\cos\theta_C \tag{4.2}$$

Where $\theta_{C\text{-}W}$, θ_C, θ_W are the contact angle of hybrid state, contact angle of Cassie-Baxter model, contact angle of Wenzel model and f_w is fraction of Wenzel state. f_w is assumed to equal to ρ* which is ratio of average density inside the cavity to bulk density of liquids. Therefore, the hybrid model can be described as follows:

$$\cos\theta_{C-W} = \rho^* \cos\theta_W + (1 - \rho^*)\cos\theta_C \tag{4.3}$$

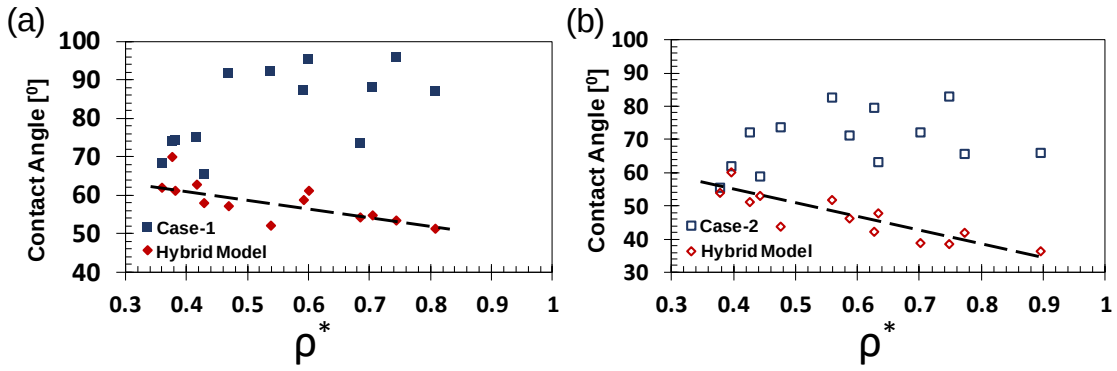

Figure 4.8. Wetting angle predictions of hybrid model and measured contact angles (a) Case 1 and (b) Case 2

Contact angle prediction of the hybrid model is presented in Figure 4.8. Hybrid model mostly underestimates the wetting angle of nanopatterned silica surfaces. Close predictions are only observed on R_{441} surfaces of the both cases. The reason of failure is that a fraction of Wenzel state is overestimated with the hybrid approach and hybrid model predicts more hydrophilic surfaces than actual ones. Therefore, approximation made by Yeh and Soong fails. When their study is investigated carefully, it is seen that they systematically vary roughness ratio of the surfaces but base of the patterns consists of two or three layers of atoms. Thus, adsorbtion of water molecules inside the cavities is underestimated because effective range of dispersion forces between atoms is assumed to be one nanometer which is why one nanometer cut off distance is employed in MD simulations. Therefore, in their case, thickness of silicon layers should be one nm, at least.

Missing layers can underestimate attraction force between water molecules and surface so density distribution in the cavities underpredicted.

4.6. Wetting Characterization of Nanopatterned Silica Surfaces

Although density deviation of inside cavity water is found to be in appropriate to establish hybrid Cassie-Baxter and Wenzel states approach, average density inside the cavity might capture effects originating from existence of corrugations so it could be considered as a tool to characterize wetting behavior of nanopatterned surfaces. Therefore, average density inside the cavity is investigated.

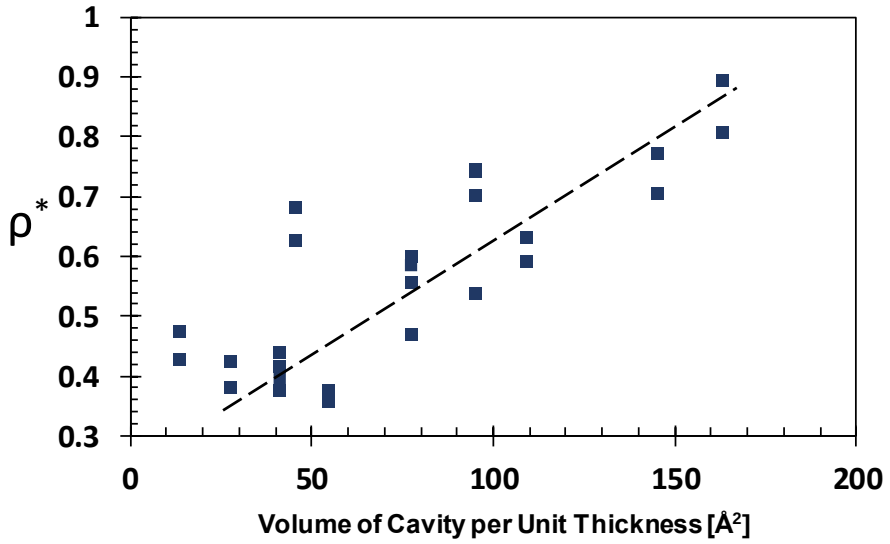

Figure 4.9. Relation between normalized cavity density and normalized work of adhesion

In Figure 4.9, normalized water density inside the cavity, ρ* is presented as a function of cavity volume per unit thickness. Since nanogrooves are designed as surface patterns, volume of cavity is presented in the form of volume per unit thickness. It can be inferred from the figure that water distribution inside cavites can be characterized as a function of cavity volume as expected. The trend suggests that for smaller cavities, density inside cavities diverges from bulk behavior. However, small deviation in densities can be observed for the same cavity volume as a result of different interaction strength between water and silica surfaces.

In Figure 4.10 relation between normalized cavity density and normalized work of adhesion is presented to investigate the effect of normalized water density inside the

cavity on change in the contact angle. As presented in equation 4.1, the term 1+cosθ is direct factor of work of adhesion so (1+cosθ) is approximated as non-dimensional work of adhesion. Furthermore, work of adhesion of each patterned surface is normalized with work of adhesion of smooth surfaces. Normalization is expressed with the expression (1+cosθr)/(1+cosθ∞) where θr and θ∞ denote contact angle of rough and contact angle of smooth surfaces, respectively. Therefore, the expression (1+cosθr)/(1+cosθ∞) shows how much deviation in work of adhesion is observed due to corrugations. Since value of the cosine function decreases as the degree increases from 0 to π, contact angle of nanopatterned surface increases as deviation in normalized work of adhesion increase. It should be stated that when surfaces have 1-layer depth density, normalized density inside cavity is less than 0.5 and for those surfaces as water distribution inside the cavity increases, more deviation from work of adhesion is observed. Moreover, it can be inferred from the Figure 4.10 that as normalized density increases change in contact angle of rough surfaces stay constant. However, huge variation in normalized work of adhesion is noted for similar density values. Two different trends can be observed as density increases and there is no common trend observed for case 1 and case 2. Therefore, an area is introduced on Figure 4.10 to show effect of normalized cavity density on contact angle and two outlier points denotes hydrophobic surfaces of case 1. After all, normalized density is found to be inefficient to characterize wetting behavior of rough surfaces.

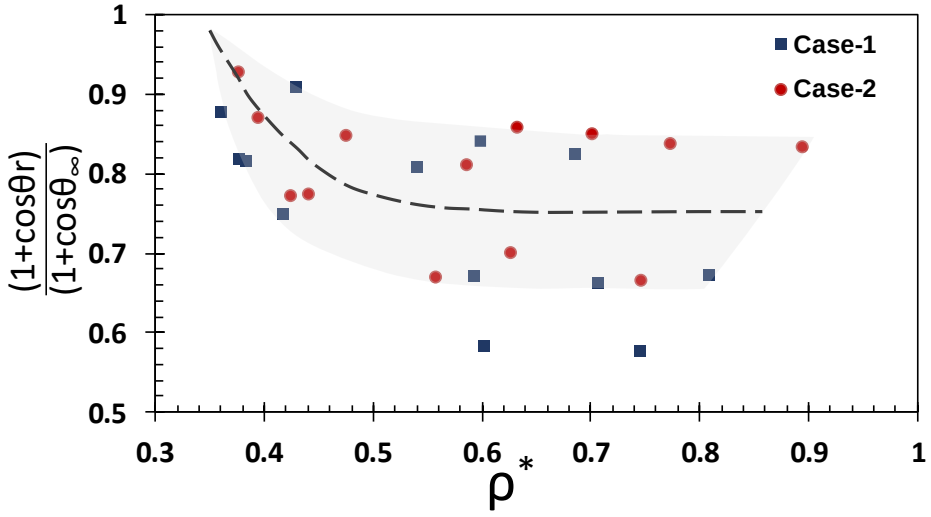

Figure 4.10. Relation between normalized cavity density and normalized work of adhesion

Although Wenzel state is observed, nanopatterned silica surfaces exhibits behavior conflicting with Wenzel model prediction as previously reported in the

literature[53,57]. Decrease in the interactions between substrate and droplet due to removed atoms from the surfaces is claimed to be one of the reason of contradictory behavior but in this study, it is presented that water adsorbtion inside is higher than the adsorption on the top of pillar so extracting atoms from surface actually increases total interaction between substrate and water due to rise in solid-liquid contact area. Therefore, removing atoms from surface, indeed, increases water adsorption inside the cavity. It is shown that to increase contact angle, more water is required to accumulate inside the cavity but that relation is insufficient in capturing wetting behavior of nanopatterned silica surfaces.

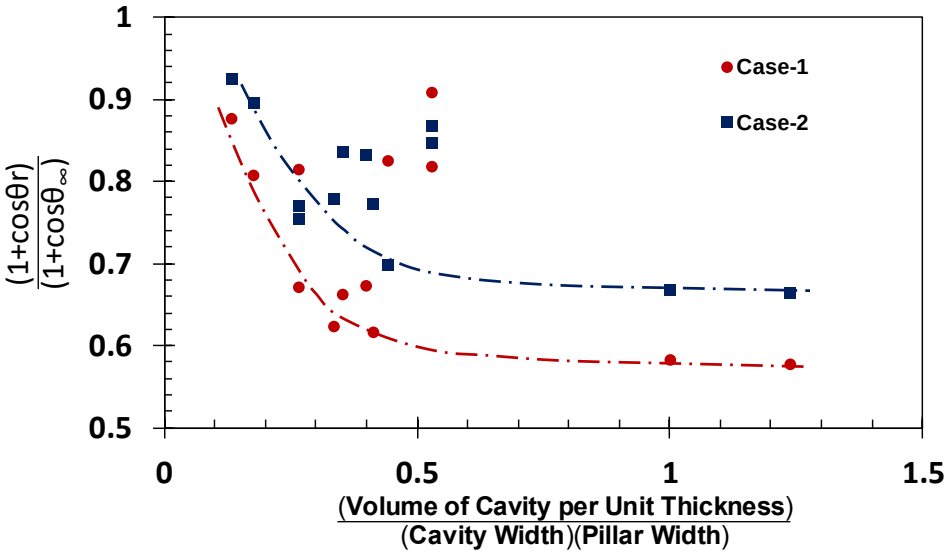

Figure 4.11. Relation between normalized work of adhesion and proposed surface parameter.

So far, it is presented that classical approaches are inadequate to predict wetting angle of patterned hydrophilic surfaces. Moreover, contact angle of a rough surface increases as cavity depth change from one layer to two layers so it can be said that increase in cavity volume lead to rise in contact angle. Furthermore, pillar width is reversely proportional with contact angle. By considering these, non dimensional surface parameter which is ratio of cavity volume to pillar width and cavity width is defined empirically to capture wetting behavior of rough surfaces. To accomplish that, change in the work done by droplet, work of adhesion rather than contact angle, is considered. In Figure 4.11, change in the work of adhesion of the surfaces as a function of the proposed surface parameter is presented. Both case 1 and case 2 follow a similar trend as the surface parameter increases. While surface parameter increases change in the contact angle increases and when surface parameter reaches 1, increase in the deviation from smooth surface stops. Moreover, maximum deviation from smooth surface depends on contact

angle of smooth surface because maximum deviation of case 1 and case 2 differs from each other. Although, proposed parameter captures wetting behavior, deviations from trendlines are observed for some surfaces and discrepancy could originate from local effects.

CHAPTER 5

CONCLUSION

Surface wetting is a very important phenomenon for interface science. It is observed because of the equilibrium in interfacial tensions on a surface and classically can be quantified by the contact angle via Young's equation. The ability to manipulate the wetting behavior of surfaces is important for a great numbers of applications. To accomplish manipulation, the main objective is to set the tension between surface and other substances and adjust it for desired characteristic. Conventionally, it has been tried to adjust surface wetting by coatings or chemicals but with the discovery of lotus effect, surface patterning became a promising tool for wetting control. Similarly, with the discovery of rose petal effect, the effect of nanoscale roughness on wetting has gained attention. However, the relation between nanoscale surface structures and the wetting behavior is not fully understood. Attempts have been made to explain effect of nanoscale roughness on wetting by considering macroscopic models such as Wenzel and Cassie-Baxter or combining these models to predict contact angle of nanopatterned surfaces but a clear explanation of the underlying mechanism behind wetting on nanopatterned surfaces is still missing.

This study aims to investigate dynamics of nano scale surface wetting. The main objective is to investigate the manipulation of the surface wetting properties by nano-scale surface structures with the help of surface structures similar to nano pillars discovered on rose petal. To accomplish our goal, molecular dynamics simulations are performed. Priorior to investigation on rough surfaces, wetting of smooth silica surfaces are studied. To find appropriate interaction parameters between water molecule and silica surfaces, ab initio calculations are performed. However, it is observed that ab initio calculations overestimate interaction strength between oxygen atoms of water molecules and silicon-dioxide which is frequently used in nano-technological applications. Thus, ab inito based interaction strength results in lower contact angle on smooth silica surface. Therefore, interaction strength between water and silica surface is calibrated with the help of wetting studies on the smooth surface. Due to variation in experimental contact angle of silica, two different wetting angles are determined and interaction parameter between

dissimilar oxygen atoms, which are oxygen of water and oxygen from silica structure, are tuned to reproduce determined contact angles.

After calibration and reproducing experimental contact angle results in MD simulations, silica surfaces are chosen systematically to investigate effect of pillar height, depth and spacing between pillars and wetting angles are measured on structured silica surfaces. β-cristobalite form of silica is determined to capture amorphous silica properties showing that sizes of surface structures are constrained by the lattice parameters. Our findings suggest that macroscale wetting models, such as Cassie-Baxter or Wenzel, fail in predicting wetting mechanisms at small scales. Although Wenzel state is observed on the nanopatterned silica surfaces, contact angle of the hydrophilic surfaces increases which is theoretically impractical in Wenzel model prediction. This shows that the underlying mechanism of nanopatterned surfaces are completely different than macroscopics counterparts even though macroscopic states are observable in nanopatterns. Furthermore, density layering inside the cavities are investigated to check applicability of mean field theories. However, no convincing connection between near interface density profiles and wetting angle is observed. Moreover, hybrid Wenzel and Cassie-Baxter model is applied to predict contact angle of corrugated surfaces but it is shown that hybrid model generally underestimates wetting angle of patterned surfaces.

Although, approximating density inside the cavity as a Wenzel fraction of hybrid model fails, it is noted that average water density inside roughness cavity could capture both pattern size and scale effects. Therefore, averaged cavity density is used to correlate wetting angle of patterned surface to surface properties. It is observed that as average water density inside the cavity converges the bulk value, contact angle of nanopatterned surface increases. However, observed behavior of wetting is constrained with naturally hydrophilic surfaces. Hence, wetting mechanism can be explained as follows; the more bulk behavior of liquid is observed inside the cavity, near interface effects diminish and effect of solid-liquid interface on wetting decreases. Meaning, less hydrophilic behavior is observed on nanopatterned hydrophilic surface and contact angle increases as water density inside the cavity increases.

Cavity volume is correlated with average cavity density to investigate wetting manipulation on nanopatterned surfaces but it is found that cavity volume partly captures wetting behavior on nanopatterned surface. Since cavity volume is a function of cavity depth and width, effect of pillar width is neglected when cavity volume is employed to characterize surface wetting. Therefore, non dimensional surface parameter composed of

cavity volume, cavity width and pillar width is proposed to characterize wetting behavior and results show that maximum contact angle changes due to surface roughness is limited. After a certain value of surface parameter, contact angle change stops. Moreover, it is found that to obtain stable contact angle values, surface parameter should be greater than 0.5.

REFERENCES

(1) Young, T. An Essay on Cohesion of Fluids. *Philos. Trans. te R. Soc. London* **1805**.

(2) Grosu, G.; Andrzejewski, L.; Veilleux, G.; Ross, G. G. Relation between the Size of Fog Droplets and Their Contact Angles with CR39 Surfaces. *J. Phys. D. Appl. Phys.* **2004**.

(3) Wang, Y.; Gong, X. Special Oleophobic and Hydrophilic Surfaces: Approaches, Mechanisms, and Applications. *Journal of Materials Chemistry A*. 2017.

(4) Jo, H.; Yu, D. I.; Noh, H.; Park, H. S.; Kim, M. H. Boiling on Spatially Controlled Heterogeneous Surfaces: Wettability Patterns on Microstructures. *Appl. Phys. Lett.* **2015**, *106* (18).

(5) Daniello, R. J.; Waterhouse, N. E.; Rothstein, J. P. Drag Reduction in Turbulent Flows over Superhydrophobic Surfaces. *Phys. Fluids* **2009**.

(6) Kalyoncu, G.; Barisik, M. Analytical Solution of Micro-/Nanoscale Convective Liquid Flows in Tubes and Slits. *Microfluid. Nanofluidics* **2017**.

(7) Barisik, M.; Beskok, A. Temperature Dependence of Thermal Resistance at the Water/Silicon Interface. *Int. J. Therm. Sci.* **2014**.

(8) Sendner, C.; Horinek, D.; Bocquet, L.; Netz, R. R. Interfacial Water at Hydrophobic and Hydrophilic Surfaces: Slip, Viscosity, and Diffusion. *Langmuir* **2009**, *25* (18), 10768–10781.

(9) Yen, T. H. Effects of Wettability and Interfacial Nanobubbles on Flow through Structured Nanochannels: An Investigation of Molecular Dynamics. *Mol. Phys.* **2015**.

(10) Yen, T. H.; Soong, C. Y. Effective Boundary Slip and Wetting Characteristics of Water on Substrates with Effects of Surface Morphology. *Mol. Phys.* **2016**.

(11) Ramos-Alvarado, B.; Kumar, S.; Peterson, G. P. Hydrodynamic Slip in Silicon Nanochannels. *Phys. Rev. E* **2016**.

(12) Neinhuis, C.; Barthlott, W. Characterization and Distribution of Water-Repellent, Self-Cleaning Plant Surfaces. *Ann. Bot.* **1997**.

(13) Wenzel, R. N. Resistance of Solid Surfaces to Wetting by Water. *Ind. Eng. Chem.* **1936**.

(14) Cassie, A. B. D.; Baxter, S. Wettability of Porous Surfaces. *Trans. Faraday Soc.* **1944**.

(15) Nguyen, C. T.; Barisik, M.; Kim, B. Wetting of Chemically Heterogeneous Striped Surfaces: Molecular Dynamics Simulations. *AIP Adv.* **2018**.

(16) Feng, L.; Zhang, Y.; Xi, J.; Zhu, Y.; Wang, N.; Xia, F.; Jiang, L. Petal Effect: A Superhydrophobic State with High Adhesive Force. *Langmuir* **2008**.

(17) Wang, J. Y.; Betelu, S.; Law, B. M. Line Tension Approaching a First-Order Wetting Transition: Experimental Results from Contact Angle Measurements. *Phys. Rev. E* **2001**.

(18) Plimpton, S. Fast Parallel Algorithms for Short-Range Molecular Dynamics. *J. Comput. Phys.* **1995**, *117* (1), 1–19.

(19) Stillinger, F. H.; Weber, T. A. Computer Simulation of Local Order in Condensed Phases of Silicon. *Phys. Rev. B* **1985**, *31* (8), 5262–5271.

(20) Van Beest, B. W. H.; Kramer, G. J.; Van Santen, R. A. Force Fields for Silicas and Aluminophosphates Based on Ab Initio Calculations. *Phys. Rev. Lett.* **1990**, *64* (16), 1955–1958.

(21) Pedone, A.; Malavasi, G.; Menziani, M. C.; Cormack, A. N.; Segre, U. A New Self-Consistent Empirical Interatomic Potential Model for Oxides, Silicates, and Silicas-Based Glasses. *J. Phys. Chem. B* **2006**, *110* (24), 11780–11795.

(22) Munetoh, S.; Motooka, T.; Moriguchi, K.; Shintani, A. Interatomic Potential for Si-O Systems Using Tersoff Parameterization. *Comput. Mater. Sci.* **2007**, *39* (2), 334–339.

(23) Van Duin, A. C. T.; Strachan, A.; Stewman, S.; Zhang, Q.; Xu, X.; Goddard, W. A. ReaxFFSiO Reactive Force Field for Silicon and Silicon Oxide Systems. *J. Phys. Chem. A* **2003**, *107* (19), 3803–3811.

(24) Jorgensen, W. L.; Chandrasekhar, J.; Madura, J. D.; Impey, R. W.; Klein, M. L. Comparison of Simple Potential Functions for Simulating Liquid Water. *J. Chem. Phys.* **1983**.

(25) Berendsen, H. J. C.; Grigera, J. R.; Straatsma, T. P. The Missing Term in Effective Pair Potentials. *J. Phys. Chem.* **1987**.

(26) Vallet-Regí, M.; Colilla, M.; Izquierdo-Barba, I.; Manzano, M. Mesoporous Silica Nanoparticles for Drug Delivery: Current Insights. *Molecules*. 2018.

(27) Barisik, M.; Atalay, S.; Beskok, A.; Qian, S. Z. Size Dependent Surface Charge Properties of Silica Nanoparticles. *J. Phys. Chem. C* **2014**, *118* (4), 1836–1842.

(28) Chen, C.; Zhang, N.; Li, W.; Song, Y. Water Contact Angle Dependence with Hydroxyl Functional Groups on Silica Surfaces under CO2 Sequestration Conditions. *Environ. Sci. Technol.* **2015**, *49* (24), 14680–14687.

(29) Sen, T.; Barisik, M. Size Dependent Surface Charge Properties of Silica Nano-Channels: Double Layer Overlap and Inlet/Outlet Effects. *Phys. Chem. Chem. Phys.* **2018**, *20* (24), 16719–16728.

(30) Leroch, S.; Wendland, M. Simulation of Forces between Humid Amorphous Silica Surfaces: A Comparison of Empirical Atomistic Force Fields. *J. Phys.*

Chem. C **2012**, *116* (50), 26247–26261.

(31) Lopes, P. E. M.; Murashov, V.; Tazi, M.; Demchuk, E.; MacKerell, A. D. Development of an Empirical Force Field for Silica. Application to the Quartz-Water Interface. *J. Phys. Chem. B* **2006**, *110* (6), 2782–2792.

(32) Cruz-Chu, E. R.; Aksimentiev, A.; Schulten, K. Water-Silica Force Field for Simulating Nanodevices. *J. Phys. Chem. B* **2006**, *110* (43), 21497–21508.

(33) Hassanali, A. A.; Singer, S. J. Model for the Water - Amorphous Silica Interface: The Undissociated Surface. *J. Phys. Chem. B* **2007**, *111* (38), 11181–11193.

(34) Fogarty, J. C.; Aktulga, H. M.; Grama, A. Y.; Van Duin, A. C. T.; Pandit, S. A. A Reactive Molecular Dynamics Simulation of the Silica-Water Interface. *J. Chem. Phys.* **2010**, *132* (17).

(35) Hasan, J.; Raj, S.; Yadav, L.; Chatterjee, K. Engineering a Nanostructured "Super Surface" with Superhydrophobic and Superkilling Properties. *RSC Adv.* **2015**, *5* (56), 44953–44959.

(36) Barisik, M.; Beskok, A. Wetting Characterisation of Silicon (1,0,0) Surface. *Mol. Simul.* **2013**, *39* (9), 700–709.

(37) Iglauer, S.; Salamah, A.; Sarmadivaleh, M.; Liu, K.; Phan, C. Contamination of Silica Surfaces: Impact on Water-CO2-Quartz and Glass Contact Angle Measurements. *Int. J. Greenh. Gas Control* **2014**, *22*, 325–328.

(38) Werder, T.; Walther, J. H.; Jaffe, R. L.; Halicioglu, T.; Koumoutsakos, P. On the Water-Carbon Interaction for Use in Molecular Dynamics Simulations of Graphite and Carbon Nanotubes. *J. Phys. Chem. B* **2003**, *107* (6), 1345–1352.

(39) Heiranian, M.; Wu, Y.; Aluru, N. R. Molybdenum Disulfide and Water Interaction Parameters. *J. Chem. Phys.* **2017**, *147* (10).

(40) Wu, Y.; Wagner, L. K.; Aluru, N. R. Hexagonal Boron Nitride and Water Interaction Parameters. *J. Chem. Phys.* **2016**, *144* (16).

(41) Ramos-Alvarado, B.; Kumar, S.; Peterson, G. P. Wettability of Graphitic-Carbon and Silicon Surfaces: MD Modeling and Theoretical Analysis. *J. Chem. Phys.* **2015**, *143* (4).

(42) Iarlori, S.; Ceresoli, D.; Bernasconi, M.; Donadio, D.; Parrinello, M. Dehydroxylation and Silanization of the Surfaces of β-Cristobalite Silica: An Ab Initio Simulation. *J. Phys. Chem. B* **2001**.

(43) Plessow, P. N.; Sánchez-Carrera, R. S.; Li, L.; Rieger, M.; Sauer, S.; Schaefer, A.; Abild-Pedersen, F. Modeling the Interface of Platinum and α-Quartz(001): Implications for Sintering. *J. Phys. Chem. C* **2016**.

(44) Shih, C. J.; Wang, Q. H.; Lin, S.; Park, K. C.; Jin, Z.; Strano, M. S.; Blankschtein, D. Breakdown in the Wetting Transparency of Graphene. *Phys. Rev. Lett.* **2012**, *109* (17).

(45) Annamalai, M.; Gopinadhan, K.; Han, S. A.; Saha, S.; Park, H. J.; Cho, E. B.; Kumar, B.; Patra, A.; Kim, S. W.; Venkatesan, T. Surface Energy and Wettability of van Der Waals Structures. *Nanoscale* **2016**, *8* (10), 5764–5770.

(46) Raj, R.; Maroo, S. C.; Wang, E. N. Wettability of Graphene. *Nano Lett.* **2013**, *13* (4), 1509–1515.

(47) Tersoff, J. New Empirical Approach for the Structure and Energy of Covalent Systems. *Phys. Rev. B* **1988**, *37* (12), 6991–7000.

(48) Tserepi, A.; Gogolides, E.; Tsougeni, K.; Constantoudis, V.; Valamontes, E. S. Tailoring the Surface Topography and Wetting Properties of Oxygen-Plasma Treated Polydimethylsiloxane. *J. Appl. Phys.* **2005**.

(49) Tsougeni, K.; Tserepi, A.; Boulousis, G.; Constantoudis, V.; Gogolides, E. Control of Nanotexture and Wetting Properties of Polydimethylsiloxane from Very Hydrophobic to Super-Hydrophobic by Plasma Processing. *Plasma Process. Polym.* **2007**.

(50) Meli, M. V.; Lennox, R. B. The Wetting of Gold and Silicon Nanoscale Arrays. *Langmuir* **2007**.

(51) Yong, X.; Zhang, L. T. Nanoscale Wetting on Groove-Patterned Surfaces. *Langmuir* **2009**.

(52) Grzelak, E. M.; Errington, J. R. Nanoscale Limit to the Applicability of Wenzel's Equation. *Langmuir* **2010**.

(53) Svoboda, M.; Malijevský, A.; Lísal, M. Wetting Properties of Molecularly Rough Surfaces. *J. Chem. Phys.* **2015**.

(54) Yen, T. H.; Soong, C. Y. Hybrid Cassie-Wenzel Model for Droplets on Surfaces with Nanoscale Roughness. *Phys. Rev. E* **2016**.

(55) Marmur, A. Wetting on Hydrophobic Rough Surfaces: To Be Heterogeneous or Not to Be? *Langmuir* **2003**.

(56) Bico, J.; Thiele, U.; Quéré, D. Wetting of Textured Surfaces. In *Colloids and Surfaces A: Physicochemical and Engineering Aspects*; 2002.

(57) Ambrosia, M. S.; Ha, M. Y. A Molecular Dynamics Study of Wenzel State Water Droplets on Anisotropic Surfaces. *Computers and Fluids*. 2018.

(58) Gonzalez-Valle, C. U.; Kumar, S.; Ramos-Alvarado, B. Investigation on the Wetting Behavior of 3C-SiC Surfaces: Theory and Modeling. *J. Phys. Chem. C* **2018**, *122* (13), 7179–7186.